Quaternary Geochronology 78 (2023) 101472

Contents lists available at ScienceDirect

Quaternary Geochronology

journal homepage: www.elsevier.com/locate/quageo

Constraining the minimum age of Daraki-Chattan rock art in India by OSL dating and petrographic analyses

Georgios S. Polymeris [a], Ioannis Liritzis [b,c,d,e,*], Ioannis Iliopoulos [b,f], Vayia Xanthopoulou [f], Robert G. Bednarik [g,h], Giriraj Kumar [h,i], Asimina Vafiadou [j]

[a] Laboratory of Archaeometry, Institute of Nanoscience and Nanotechnology, NCSR "Demokritos", 15310-Ag. Paraskevi, Attika, Greece
[b] Henan University, Key Research Institute of Yellow River Civilization and Sustainable Development & College of Environment and Planning & Institute of Capital Civilization & Cultural Heritage, Henan, Kaifeng 475001, China
[c] European Academy of Sciences & Arts, St. Peter-Bezirk 10, A-5020 Salzburg, Austria
[d] The University of Edinburgh, School of History, Classics and Archaeology, College of Arts, Humanities & Social Sciences, Dept. of Archaeology, 4 Teviot Pl, Edinburgh EH8 9AG, Scotland, UK
[e] Rhodes University, Department of Physics & Electronics, PO Box 94 Makhanda (Grahamstown), 6140, Eastern Cape, South Africa
[f] University of Patras, Department of Geology, Rio Patras 265 04, Greece
[g] International Federation of Rock Art Organizations, P.O. Box 216, Caulfield South, Melbourne, Vic, 3162, Australia
[h] International Centre for Rock Art Dating, Hebei Normal University, Shijiazhuang, China
[i] Rock Art Society of India, Faculty of Arts, Dayalbagh Educational Institute, Dayalbagh, Agra, 282 005, India
[j] University of the Aegean, Lab. of Achaeometry, Department of Mediterranean Studies, 1 Demokratias Str, Rhodes, 85132, Greece

ARTICLE INFO

Keywords:
Equivalent dose
Dose rate
Mineralogical
Quartz-arenite
Single aliquot regeneration
Sediments
Cathodoluminescence
Microscope
Mineral
Exfoliation
Petroglyphs

ABSTRACT

Ongoing work in Daraki-Chattan cave, India, has revealed important Paleolithic rock art (petroglyphs) in the form of cupules. The site is rich in stone tools of Acheulian industry to Oldowan-like industry including several hammerstones. The present investigation concerns a further detailed methodological and complementary approach for dating a quartz-arenite sandstone clast from just above the lowest exfoliated cupule, combining surface luminescence chronology with petrography. The optically stimulated luminescence equivalent dose profiles versus depth from quartz were studied to date this clast. Two different dose-depth profiles were measured spanning to 28 mm depth, one natural depth profile and one for a sample following exposure to daylight for nine months. Equivalent dose versus depth profiles indicate bleaching in several millimeters. Varied spatial luminescence response, its effect on the luminescence-depth profiles and interpretation to circumvent minor anomalies are fully discussed in terms of non-luminescent/dull faint minerals, coating, and inhomogeneous distribution of feldspars. Thin section analysis was performed using both optical and cathodoluminescence microscopy. The former indicates mineral origin, distribution and size with dominance of monocrystalline quartz grains that makes rock type classified to a typical quartz sandstone (arenite); the latter identifies blue- and dull cyan-luminescent quartz crystals and recognizes luminescent minerals centers. Three additional micro-samplings were performed for X-ray and scanning electron microscopy analysis on specific points of the profile for minerals and chemical elements. The method followed and dose profiles from the present buried sandstone, suitably discussed, provided an average date for at least two burial sun exposure histories of the fallen stone piece of around 46 ka and 71 ka before current era, providing a constrained *terminus post quem* for the exfoliated clast from the cave wall with petroglyphs.

1. Introduction

The absolute date of carved rock art (petroglyphs), and their complex classification and interpretation, is a fast-developing topic in archaeological and Quaternary contexts that has attracted worldwide attention (MAA, 2017; Bednarik and Li, 1991). Hence auditable rock art dating, the unearthed archaeological data, and a long term of various environmental impacts are all essential components of scientific rock art

* Corresponding author. Henan University, Key Research Institute of Yellow River Civilization and Sustainable Development & College of Environment and Planning & Institute of Capital Civilization & Cultural Heritage, Henan, Kaifeng 475001, China.
E-mail addresses: g.polymeris@inn.demokritos.gr (G.S. Polymeris), liritzis@henu.edu.cn (I. Liritzis).

https://doi.org/10.1016/j.quageo.2023.101472
Received 2 November 2022; Received in revised form 13 September 2023; Accepted 25 September 2023
Available online 26 September 2023

research.

Within the topic of luminescence dating, the novel version of surface luminescence dating (SLD) has been introduced to date stone surfaces of archaeological monuments by Liritzis (1994a, b), as long as the luminescence signal has been reset due to exposure to solar radiation. Any electron re-trapping in the crystal lattice traps of the minerals (quartz and feldspar) that constitute the stone can be erased due to some later sun bleaching (Liritzis, 2022; Liritzis et al., 2020a, b). Thus, SLD was also developed to derive exposure, burial ages, and hard-rock erosion dates (Smedley et al., 2021; Brill et al., 2021; Brown and Moon 2019; Ageby et al., 2022; Chapot et al., 2012; Galli et al., 2020). Thus, for a previously steadily exposed stone surface to sunlight, following a fall and burial into the ground sediments these traps are gradually refilled by environmental radiation derived from natural radioisotopes in the stone's context.

In contrast, for a long-standing stone surface in sunlight (e.g. rock art surfaces), the bleached luminescence in the stone's inner parts is a function of a) the depth below its surface, b) the time the surface has been exposed to sunlight and c) the intensity of the sunlight (Liritzis and Galloway, 1999; Laskaris and Liritzis, 2011; Liritzis and Vafiadou, 2015; Liritzis et al., 2017). Of course, lithology might also affect the bleaching of the minerals (Ou et al., 2018). The reminiscent luminescence on a rock surface as a function of depth is described by a mathematical function that includes the age or sun-exposure time from the time of block cut stone to present (Laskaris and Liritzis, 2011; Sohbati et al., 2012; Liritzis et al., 2017). The daylight penetrates a fresh stone surface to a depth ranging between 5 and 15 mm below the surface, depending on the kind of rock lithology and exposure time (Laskaris and Liritzis 2011; Sohbati et al., 2015; Liritzis et al., 2017).

The application of the SLD method to rocks is a fast-developing absolute dating methodology built up on past published reports (Habermann et al., 2000; Greilich and Wagner, 2009; Laskaris and Liritzis 2011; Sohbati, 2013; Liritzis et al., 2013a,b; 2013c, 2017); however, this technique was further developed, not only for dating construction masonries but also stones exposed to sunlight and later buried with one or more exposure-reburial histories on applications and mathematical modelling. Readers are referred to recent articles (Gliganic et al., 2019; Freiesleben et al., 2015; Sohbati et al., 2012; Sellwood et al., 2022; Liritzis et al., 2010, 2015) as well as reviews on the topic (Scarre, 2010; Liritzis, 2011).

The present work concerns a methodological approach of dating a selected quartz-arenite clast (DC-3) from an excavated profile at the entrance of Daraki-Chattan cave in central India. The cave is located in the Indragarh-Chanchala Mata plateau, north of Bhanpura in Madhya Pradesh, which is surrounded by steep escarpments (Fig. 1a). The two cave walls are densely covered with about 500 cupule petroglyphs (Kumar and Krishna, 2015; Krishna and Kumar, 2016; Bednarik et al., 2005). However, at the entrance, insolation has caused the exfoliation of the rock art on about 7–10 cm thick slabs. Expecting to find these slabs in the sediment below, it was excavated and 28 cupules on slab fragments were indeed recovered throughout most of the 2.5 m deep sediment below the sloping floor of the cave. The upper half of the sediment contained numerous Acheulian stone tools, which even occurred at the surface. Therefore, we endeavored to determine how far the exfoliated rock art extended down the cultural sequence. As it continued well into the Mode 1 (pre-Acheulian) lower half of the sequence (layers 4, 5 and 6 in Fig. 1b), it should be of this chopper-dominated industry (Bednarik et al., 2005). The Indian Acheulian tends to fade out about 200 ka ago (Raghvan et al., 1989; Szabo et al., 1990; Mishra, 1992; Paddayya, 1991; Korisettar, 2002) and is preceded by an Oldowan-like chopper industry (the age of which remains controversial; Bednarik et al., 2005).

This raised the issue of dating this Lower Paleolithic rock art but attempts to use various methods failed. We decided to apply surface luminescence dating, but the exfoliated cupule slabs had all been exposed to light during excavation. We therefore re-opened the excavation trench (which had been filled in) and secured clast DC-3 under complete exclusion of light (exposing it at night under a black plastic tent) from close to the location of the lowermost exfoliated rock art fragment (i.e., ca. 18 cm above it and distanced <20 cm horizontally). Thus, DC-3 would provide an effective minimum age of the burial of the lowest cupule slab.

The stratigraphical attribution of the exfoliated cupules to a Mode 1 industry underlying significant Mode 2 (Acheulian) deposits also implies that the Daraki-Chattan rock art is earlier than any of the other proposed Lower Paleolithic cupules of world. They are all in Africa: those on the decorated quartzite pavements of Potholes Hoek and Nchwaneng in the southern Kalahari, South Africa (tentatively placed at 410 ka ago; Beaumont and Bednarik 2013), and those on an excavated sandstone slab from the Lower Sangoan of Tai Island, Sudan (dated 200 ka ago; Van Peer et al., 2003).

Earlier optically stimulated luminescence (OSL) dating in Indian caves included a) three sediment samples from Daraki-Chattan and b) four samples from Bhimbetka. All these provided results that were inconclusive in that they included a major inversion at the latter site, and Holocene dates for Acheulian tools at the former site (Bednarik, 1993; Bednarik et al., 2005). OSL dating was later performed to another exfoliated sandstone fragment with code name DC-LIR-1 from Boulder E which derives from a shallower depth of the stratigraphy (Fig. 1b) (Liritzis et al., 2019). The present work is a follow up of this earlier work in this cave.

The ultimate goal of the present study is the dating investigation of a quartz-arenite clast (laboratory name DC-3) that was derived from the excavation trench at a depth around 2 m in front of the cave's entrance and was recovered there stratigraphically above and below pieces bearing cupules and grooves.

The rationale is the investigation of equivalent dose versus depth of two profiles (from the weathered top, extending down to a depth of nearly 3 cm, see, Liritzis et al., 2013a; 2013c, 2017, 2019), and conducting meticulous petrographic investigation with elemental, microscopic and spectroscopic techniques to achieve a reliable dose and dose rate result. One dose profile concerns the original sample that was not exposed to sunlight during and following collection, and another dose profile results from an experimental test of the same stone sun-bleaching for nine months, introducing an extended methodological approach regarding possible burial-bleaching histories. The specific aim of the present study is to attempt a direct dating of the burial of the clast which gives a *terminus post quem* for the production of the nearby petroglyph.

2. Methods

2.1. OSL analysis

2.1.1. On-site sampling

The sample with laboratory reference name DC-3 is the subject of the present work; it is a quartz-arenite sandstone (Fig. 2a) originating from a low level of the excavation (Fig. 1b). It was covered by around 20 cm of sediment, and was collected under 100% light-proof conditions, as sampling took place during night. Images "before" and "after" the sample collection that refer specifically to the context of the DC-3 are shown in Fig. 2b. The sample was recovered from ~ 2 m below ground surface,near the base of the sediment column.

It is a clast in the sediment; its only relevance to the dating of rock art is that it occurred slightly above the lowest exfoliated cupule fragment and it wasn't exposed to light. This specific sample was collected from immediately to the right of the slab with the cupule; therefore, it is reasonably expected to be younger than the cupule, one of thirty found in the excavation (Fig. 2). Indeed, this refers to a conservative exfoliation time, so it provides merely a minimum age of the cupule. All cupules are probably roughly of the same age, but they exfoliated at different times (from Lower to Middle Palaeolithic times) and all we can know is when they were deposited in their respective locations.

Macroscopically it consists of two, somewhat flattened surfaces

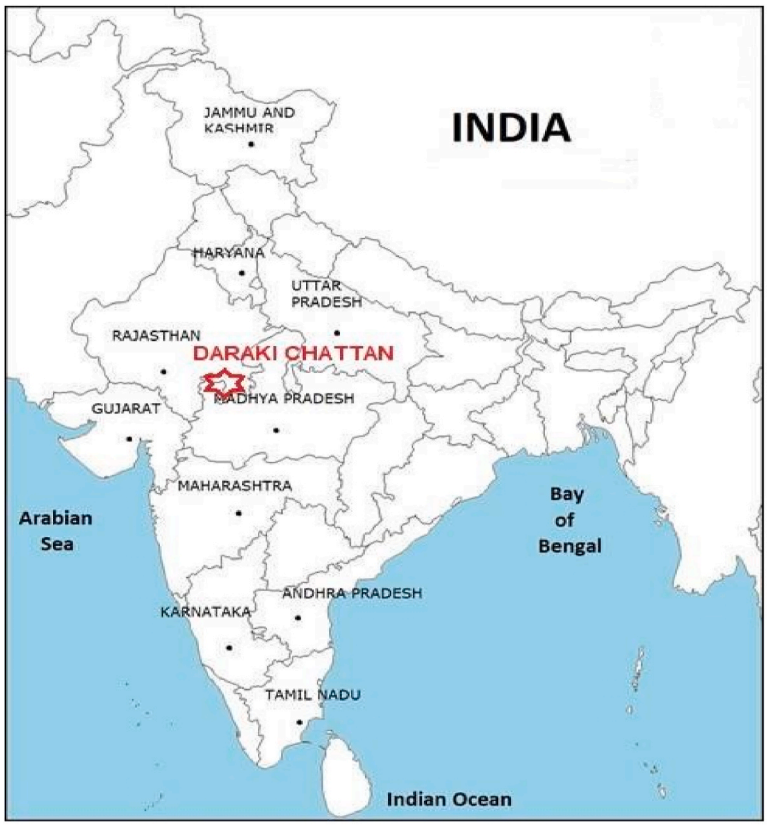

(A)

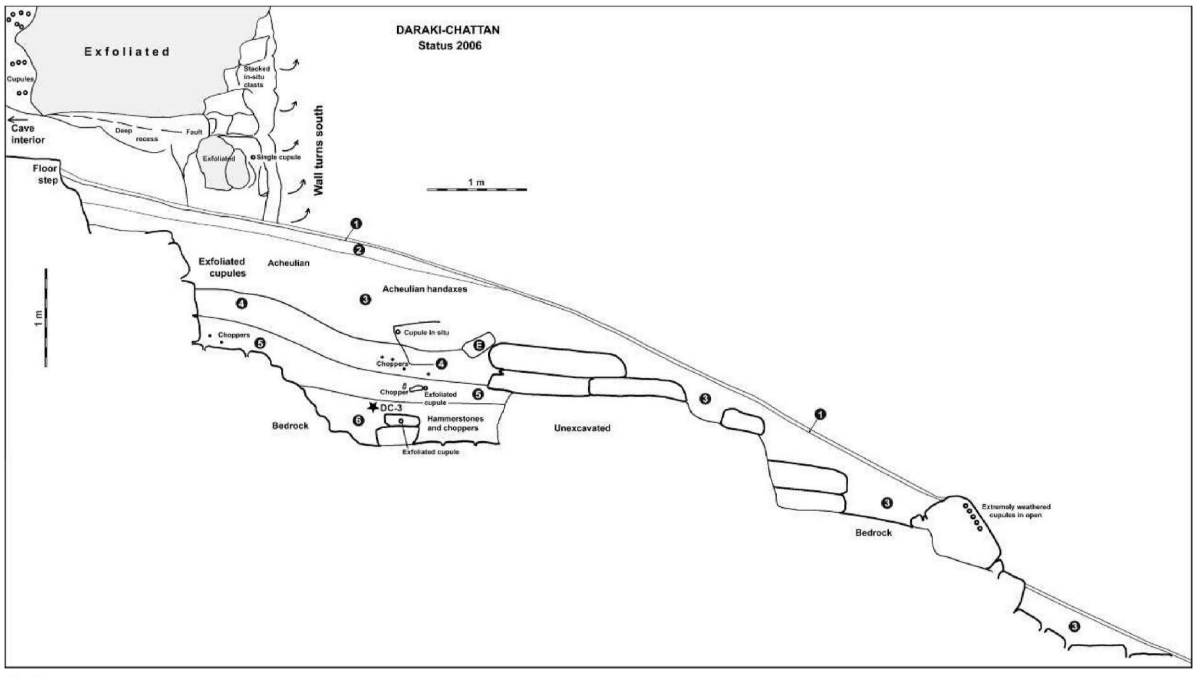

(B)

Fig. 1. **(a)** Map of India indicating the site of the present study, **(b)** The section of Daraki Chattan rock art, stratigraphy and cave entrance. The location of rock sample DC-3 is indicated by a star, at a depth of about 2 m next to the number 6 in black circle. Exfoliated cupules and boulders bearing cupules and grooves were found buried in the sediment, as well as Acheulean and Mode 1 tools. Numbers 1–6 in black spots represent layers (Bednarik et al., 2005; their Fig. 26).

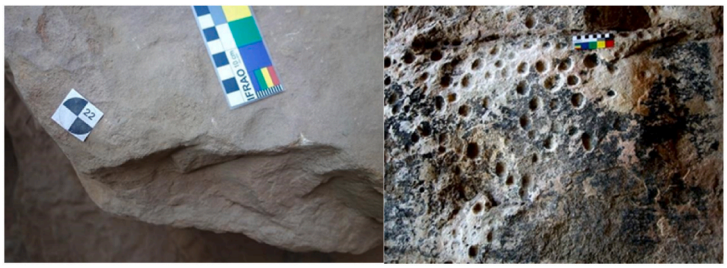

(A)

(B)

Fig. 2. **(A)** Cupule on very large rock slab excavated in situ in lower part of layer 3, as indicated in Fig. 1b, and adjacent in situ cupules (right); **(B)** Position of DC-3 sandstone clast, shown by black dot; left: before sampling, middle: after sampling, collected piece between the lower two 3D markers, and right: the context, about 2 m below ground. The markers are for 3D visualization.

weathered with rich reddish oxides (Fig. 3a); however, the inner part of the sample was intact, without weathering tracks. It is not known which one of the flattened areas was exposed to daylight. Sampling was performed perpendicular to these aforementioned surfaces of interest to at the slab's profile (from the weathered top extending down to a depth of nearly 3 cm). The NaI scintillometer gamma-ray readings were taken by inserting the probe in the hole left by the removal of the sample, as per photo Fig. 2b left (see also color marker left and middle of Fig. 1b). In a radius of ~30 cm around sample DC-3 is large quartzite clasts dominated gravel 70% and sand 10%.

2.1.2. Laboratory subsampling and preparation

The initially retrieved rock art sample was kept in dark since the collection time from the excavation in India. Under red light room conditions, the rock sample was cut vertically into two sub-cores. For the first sub-core, abrasion occurred immediately after cutting the rock art sampling into two pieces. The second sub-core, before slicing, was exposed to sunlight in Rhodes Island, Greece, over a total length of 9 consecutive months. For both sub-cores, the surfaces of the rock fragments (about 4 cm × 3 cm × 3 cm) were cleaned with diluted HCl. Each surface was then lightly abraded using a medium coarse rasp; grains from 1 cm^2 area were abrades, starting at the top surface and abrading down to the bottom surface, in 1 mm increments up to a depth of ~30 mm (40–45 subsamples). Gentle removal of grains in closely spaced intervals along the profile was made using 50 rubs per layer of varying thickness in mm. Despite the fact that the sampling depth was the same for both cores, a total of 43 layers was recovered for the rock art and 48 layers for the bleached analogue) (Fig. 3a and b), corresponding to a sampling rate of about 0.7 mm/layer to the best-case scenario. The size of the grains had an average of (400 ± 10) μm (medium to coarse sand). The abraded grains of gentle plating of all subsamples were then treated with acetone. No acid treatment was made, thus alpha particle dose-rates are included in the total dose rate. Throughout the samples' length, variation of physical properties, such as texture and color, were monitored. Table 1 presents the physical properties of each sub-sampling area. The top and bottom sides were easier to rub while intermediate layers more difficult, as shown in Table 1 above. This softy top and lower parts may be caused from the weathered exposure of the former surface with the groove and the sedimentary environment after the fall for the latter. The obtained grains were cleaned with acetone, put in aluminum discs and further measured using the single aliquot regenerative OSL protocol. Consequently, for dose-rate evaluation the two radiation components of alpha particles and beta particles dose-rate from the surrounding environment of grains in the rock were accounted plus the gamma rays-dose rate from the adjacent volume of sediment and clasts in a radius of approximately 30 cm.

The functional behavior of bleached luminescence from the outer surface to the inner parts of the rock is worth examining with the aim of extracting information regarding the dose variation as a function of depth and sun exposure time. Thus, the nine months sun exposure was selected to examine and confirm the behavior of equivalent doses versus depth in the rock specimen regarding bleaching. That is what shape such a profile can take, and how useful such a ratio profile can be in informing us on the bleaching depth. Hence, in November 2019, part of the DC-3 sample was covered with aluminum foil, leaving the upper side exposed to sunlight for nine months (14 Nov. 2019–14 Aug. 2020).

2.1.3. Apparatus

OSL signals were measured using a RISØ TL/OSL DA-15 luminescence reader following irradiation to beta radiation at ambient temperature using a $^{90}Sr/^{90}Y$ beta source at a dose rate of 0.083 Gy/s determined for quartz with a size of 90–140 μm. All measurements were carried out in nitrogen atmosphere and the luminescence light was detected by an EMI 9235QA photomultiplier tube through a 7.5 mm Hoya U-340 filter (transmission band between 290 and 370 nm). Preheating was carried out in a nitrogen atmosphere using a slow heating rate of 2 °C/s, to avoid significant temperature lag (Kitis et al., 2015). All OSL measurements were carried out in the continuous-wave (CW-OSL hereafter) mode for 150 s at 110 °C, using a set of blue LEDs of wavelength 470 ± 20 nm operated at 36 mW/cm^2 maximum optical power density at the sample position (90% of the maximum stimulation intensity). For infrared stimulations, an infrared solid-state laser (880 nm,

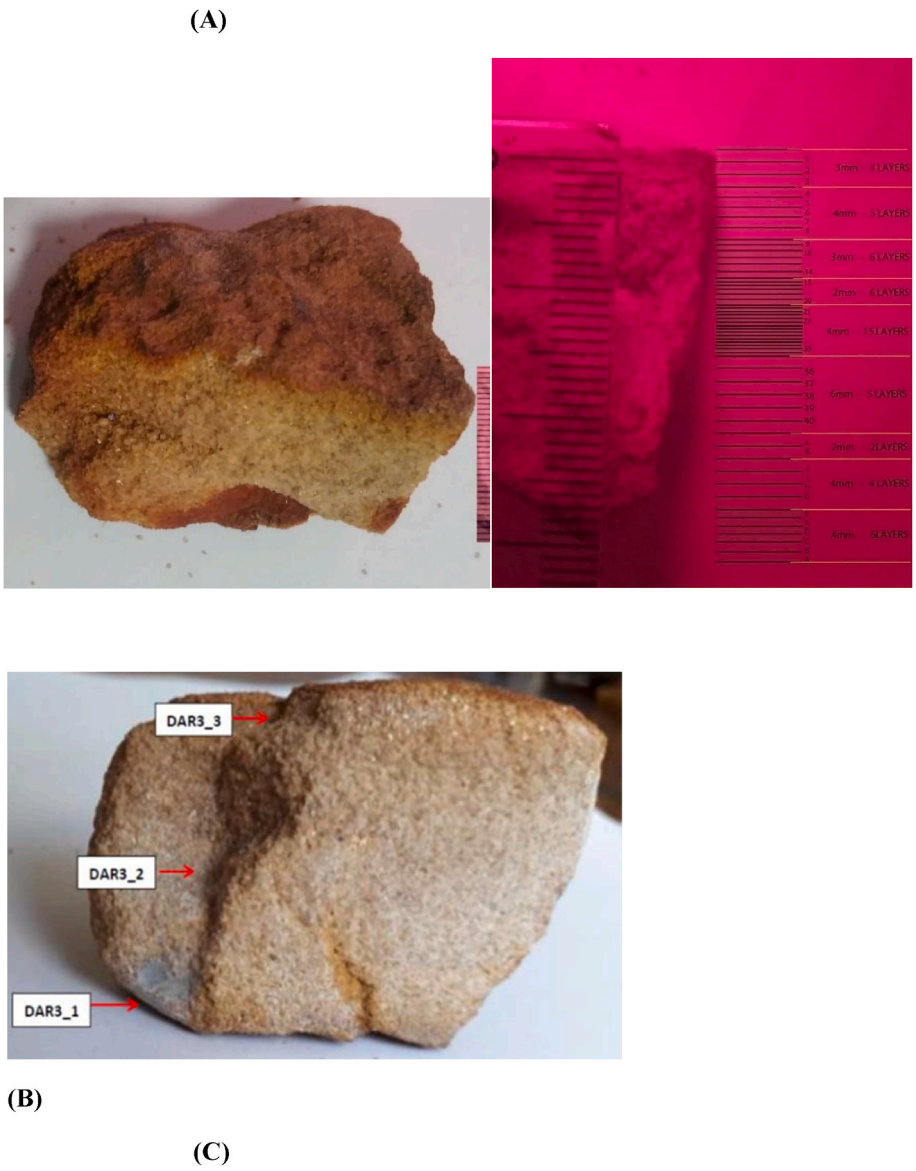

Fig. 3. Sampling for OSL: **(a)** the DC-3 sandstone sample with reddish weathered surfaces and the main stone body in yellow, and besides the profile of layers removed, **(b)** Macroscopic appearance of the sample DC-3. The labels DAR3-1, 2,3, indicate the three qualitatively different subdomains where further micro-sampling has been performed for mineralogical and chemical composition under X-ray techniques (X-ray powder diffraction and X-ray fluorescence analysis).

Table 1
Layers sampled, thickness, color and hardness of the various layers from the two samples.

Buried Clast	Properties	Bleached analogue	Properties
13.5 mm (layers 1–17)	Soft, reddish brown weathered surfaces	5.5 mm (layers 1–7)	Soft, reddish brown weathered surfaces
6 mm (layers 18–33)	Hard, dark yellow surfaces	7.0 mm (layers 8–22)	Hard, dark yellow surfaces
7.9 mm (layers 34–47)	Soft, yellow surfaces	8 mm (layers 23–37)	Hard, yellow surfaces
		7.5 mm (layers 38–49)	Soft, yellowish white surfaces

FWHM 75 nm, maximum power 135 mW/cm^2) was used, at steady stimulation intensity (80% of the maximum stimulation power) (Bøtter-Jensen et al., 2000). In a given aliquot, 10 mg (±5%) of grains having particle sizes in the range of 140–200 μm were used. The low heating rate does exclude interference from the 110 °C TL trap as the stimulation temperature is 110 °C instead of 125 °C.

2.1.4. OSL measurements, protocols and technical details

In the present study equivalent doses (ED) were measured applying the SAR OSL protocol (Murray and Wintle, 2000), following the modifications suggested by Banerjee et al. (2001) for polymineralic/mixed quartz-feldspathic samples. Table 2 summarizes the steps of the applied protocol. The procedure is similar to the double SAR procedure, containing additional SAR steps in order to minimize the need for chemical separation which is quite important in cases where the sample quantity is limited. Nevertheless, only the blue stimulated luminescence signal is being used. This approach was used primarily for the two reasons listed below (a) the low mass quantity of each sample-layer, that made the isolation of the dominant quartz mineral rather difficult and (b) for comparison with the previous results of our group (Liritzis et al., 2019), because in that latter pilot work the same protocol was applied.

In any version of the SAR OSL protocol, the signal intensity of an

Table 2
Steps, actions, comments, and technical specifications on the (double) SAR protocol of the present study.

Step no	Action	Comments & Technical Specifications
1	Regenerative dose, D_i	*D_1=0 Gy (Natural), D_2-D_7 Regenerative doses (8, 15, 35, 50, 75 and 120 Gy), D_8=0 Gy (Recuperation test), D_9= D_3 (Recycle point)*
2	Preheat	*Duration 10 s, Temperature 200 °C*
3	IR stimulation	*Duration 150 s, Temperature 30 °C: to deplete signal contamination from non-quartz minerals*
4	CW-OSL measurement	*Duration 100 s, Temperature 125 °C: Natural & regenerative OSL measurement L_i from quartz*
5	Give test dose, D_i	D_t=15 Gy
6	Cut-heat	*Duration 0 s, Temperature 180 °C*
7	IR stimulation	*Duration 50 s, Temperature 30 °C: to deplete signal contamination from non-quartz minerals*
8	CW-OSL stimulation	*Duration 100 s, Temperature 125 °C: Test dose OSL measurement L_t from quartz*
9	Return in 1 for a fresh sample	*Each measurement cycle was repeated for (at least) 2 different aliquots.*

aliquot of extracted grains is recorded at first without attributing any dose in step 1 (called natural OSL, NOSL hereafter); then the same aliquot is subjected to a series of subsequent laboratory irradiations with a calibrated radiation source and OSL measurements. Each OSL measurement removes electron charge from the excited levels and the laboratory irradiation regenerates quartz's ability to yield luminescence. This technique enables the use of a limited quantity of sample. Six different regenerative doses were applied incrementally in order to construct the dose response curve, along with a zero-dose check for the extent of thermal transfer and a repeat dose point (15 Gy) in order to examine the adequacy of the test dose sensitivity correction procedure. Infrared stimulation was applied in order to deplete the non-quartz signal; thus the main measurement (L_i) is obtained during step 4. After each regenerative dose, the sample was preheated to remove unstable OSL components; this preheating temperature was selected according to preliminary preheat plateau test; an example is presented in the upper plot of Fig. 4, where the variation of three parameters, namely ED, recuperation as well as recycling ratios are plotted versus the preheating temperature.

Sensitivity changes were both monitored and corrected with the aid of a test dose, delivered after each regenerative, natural, and zero dose OSL measurement following a cut-heat temperature of 180 °C for the same reason as the preheat treatment. The ED is calculated by comparing (using interpolation) the NOSL normalized signal to the regeneration signals induced by the increasing regenerative doses. All the tests required to guarantee trustworthy equivalent dose estimation were performed, including recuperation, recycling ratio and isolation of OSL signal from quartz (Fig. 4). For more details on the SAR OSL technique, the readers could refer to (Liritzis et al., 2013a) and (Li and Li, 2019).

Optically stimulated luminescence signals were measured and equivalent doses were calculated for two different cases, namely for each sub-piece of the rock art sampling. The same protocol was applied for both data sets. In order to make the reading of the article easier, the first data set will refer to the buried rock art set while the second data set will be termed as bleached analogue. Aliquots were accepted for OSL analysis if they met the following criteria.

I. Detectable net natural test signal greater than three sigma above the background signal (lower plot of Fig. 4)
II. Recycling ratio values within 15% of unity and recuperation values less than 20% (Figs. 4 and 5)
III. Sensitization correction (average value within 1 ± 0.2 over all test doses for each sample)
IV. Depletion of the IRSL signal within 150 s of stimulation (in the presence of the corresponding signal). Based on these four aforementioned criteria, a tiny fraction of aliquots has been considered as outliers. For the number of aliquots that were used for the calculation of the equivalent dose of each layers, the following comments stand:

1. The equivalent doses (of all 49 layers) that were calculated in the present study lie in a wide range, between 10.36 and 92.88 Gy for the buried rock art. It is quite interesting to note that in the case of the bleached analogue, the minimium ED corresponding to the bleached edge of the sample is not zero Gy, being calculated around 3.5 Gy, implying a residual due to charge transfer in agrrement to recuperation tests, while the maximum ED value for the bleached analogue does not exceed 82 Gy.
2. All ED values were calculated with high precision, namely low error values. Error values are even lower for the buried rock art.
3. For the majority of the aliquots for the SAR analysis, saturating exponential expressions were used for fitting dose response curves. A typical example of such a dose response curve is presented in the inset of lower Fig. 4 using the normalized signal, L_i/L_t, for each regenerative dose. For the remaining aliquots, the dose response was fitted using linear equations, mostly due to low ED values.
4. Even though recuperation values met the aforementioned criteria, it is quite interesting to note that the values of the bleached analogue are systematically higher compared to those of the archaeologically bleached data set. This latter feature could be easily revealed from Fig. 5 where the recuperation values are plotted versus depth for both samples. High recuperation values indicate phenomena of charge transfer, which in turn could be attributed to the bleaching effect.

2.2. Dose rate determination

Thick source alpha counting was used for the determination of the uranium and thorium content. The a-counter used is an ELSEC low level alpha-counter 7286 with an EMI 6097 B PM tube, and ZnS(Ag) on mylar film, incorporating an internal 6502 microprocessor and properly calibrated (Liritzis and Vafiadou, 2012). The U-238 and Th-232 are measured using the "pairs technique" (Aitken, 1985, 1998). The rock sample was crushed and ground down in agate mortar, the granulates sieved in particles finer than 90 μm and dried in a drying oven for 24 h at 60 °C to remove any humidity. Prior to the reading the pulverized samples were transferred in specially designed containers and sealed for 4 days to allow build-up of gaseous Radon (Rn-222, half-life $t_{1/2} = 3.823$ days) (Aitken, 1985, 1998; Liritzis and Vafiadou, 2012).

The grains are of medium to coarse size, the predominant grain size had a mean of 400 ± 10 (1σ) μm (see Fig. 3). The a-efficiency factor is taken equal to 0.10 ± 0.02 applied for medium to coarse-grained quartz (Olley et al., 1998). No acid treatment was performed. Attenuation coefficients for alpha and betas per isotope are taken from Durcan et al. (2015, their Figs. 2 and 3); for $\varphi = 400$ μm on average for U and Th it is Da*0.1. The respective attenuation for betas per isotope on average are: for U and Th × 0.80, K: × 0.90, Rb: × 0.70. Considering the coating layer in quartz of 8–10 μm the average U and Th attenuation for alphas and betas is getting lower to about × 0.70 (Liritzis et al., 2019). The cosmic-ray dose-rate 0.20–0.30 mGy/a is not included in the NaI (Tl) reader. Cosmic rays dose rate for latitude 24°N and longitude 75°E and altitudes 450 m a.s.l. is estimated as 0.30 mGy/a. An average value of 0.25 ± 0.05 Gy/ka was used.

The total dose-rate can only be approximated under contemporary burial status, that is found ~200 cm below ground surface (Fig. 1b). Due to the inhomogeneous context no costumed software is prudent to use and each separate radiation component is meticulously evaluated (Liritzis et al., 2013b; Liritzis, 2022).

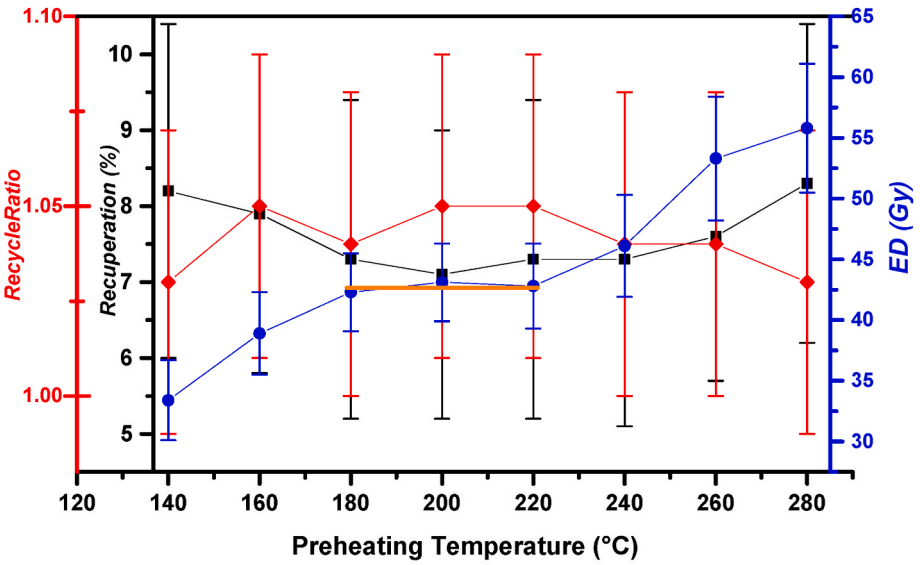

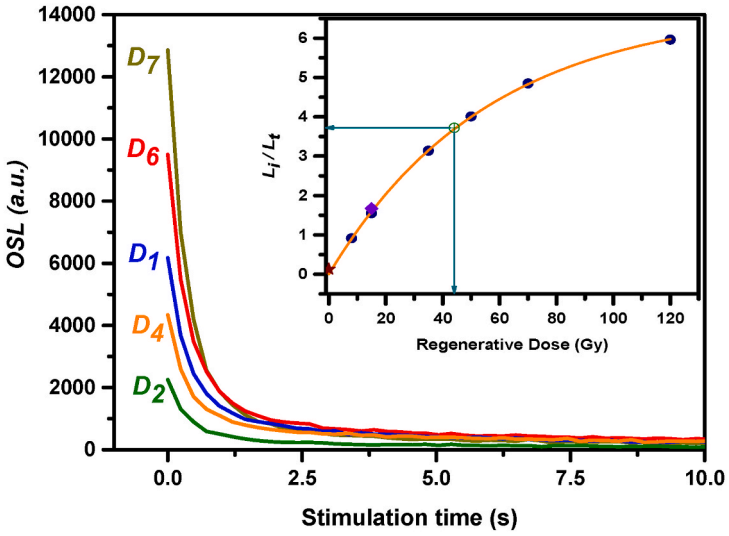

Fig. 4. Upper plot presents the equivalent dose (blue dots), the recycling ratio (red diamonds) and the recuperation values (black squares) as a function of the preheating temperature measured for an inside layer; an ED preheat plateau is yielded within 180 and 220 °C (line). The stimulation temperature of 200 °C was selected due to being in the middle of this plateau as well as due to the lowest corresponding recuperation value. Lower plot presents OSL signals following a selection of regenerative doses (according to Table 2). Just the initial 10 s of stimulation are presented for the sake of clarity. The inset presents a typical SAR growth curve, measured for an aliquot selected from the same layer. ED value (43.1 Gy) is provided by the interpolation of the natural normalized OSL signal (open dot) onto the dose response growth curve (line) resulting from the measurement sequence (filled dots). The dose response curve passes through the origin (filled star, recuperation point); Filled diamond represents the recycle point value.

2.3. Mineralogical, chemical and structural analysis

2.3.1. Handling of the sample

For the petrographic analysis the rock sample was cut using a diamond saw, following a direction perpendicular to the outer, reddish colored surface rich in iron oxides (upper part of the sample in Fig. 3), to obtain a rectangular slab for preparing a thin section. For a thorough examination of any possible compositional variability existing across the sample, three different micro-samplings were further performed using a diamond tipped micro-drilling machine in subdomains of the sample where macroscopic differences were conspicuous (points DAR3_1, DAR3_2, DAR3_3; indicated by labels in Fig. 3c above). The material obtained from the three micro-samplings as well a whole sample aliquot was powdered using an agate mortar, to evaluate their mineralogical and chemical composition under X-ray techniques (X-ray powder diffraction and X-ray fluorescence analysis, respectively).

2.3.2. Equipment and type of analysis

The mineralogical and petrographic characteristics of the studied sample were obtained through thin section preparation and optical microscopy at the Laboratory of Mineral and Rock Research, Department of Geology, University of Patras, Greece – LMRR. Microscopic observation of the thin sections was performed using a Zeiss AxioScope, along with a polarizing microscope equipped with a Jena ProgRes C3 video camera.

For compositional analysis, X-ray diffraction (XRD) was studied at the premises of LMRR. In particular, an aliquot of the studied sample was ground to <10 μm powder by using an agate mortar and was subsequently analyzed under a BRUKER D8 Advance X-Ray diffractometer, with Ni filtered Cu Kα radiation, operating at 40 kV/40 mA. The

interpretation of the acquired diffractograms and mineral identification was performed using DIFFRACplus EVA software (Bruker-AXS, Madison, WI, USA) based on the International Centre for Diffraction Data Powder Diffraction File (2006). The scanning area covered the interval 2°–70° 2θ, with a scanning angle step of 0.015° *2θ* and a time step of 0.1 s (Iliopoulos et al., 2011).

The material remaining following the preparation of thin section was analyzed by means of X-ray fluorescence coupled with energy dispersive spectroscopy (XRF–EDS) performed at Laboratory of Electron Microscopy and Microanalysis, School of Natural Sciences, University of Patras, Greece – LEMM, using a NEX CG, Rigaku system with an X-ray tube with Pd anode, working under a tube power of 50 W (50 kV to 2 mA). It is equipped with 5 secondary targets and a silicon drift detector (SDD). Standardless analysis performed using RPF-SQX (Rigaku profile fitting – spectraquant X) software with a fundamental parameters method for accurate quantification combined with full profile fitting method.

The analytical techniques that were applied to investigate the internal nature of the rock art piece also include scanning electron microscopy coupled with energy dispersive spectroscopy (SEM–EDS) for both compositional and morphological analysis of the sample. A JEOL 6300 scanning electron microscope equipped with an EDX spectrometer at LEMM was used for the main characterization; all measurements were performed on a carbon coated polished thin section under backscatter mode. The measurements were performed non-invasively and on intact surfaces using a removable, conductive carbon tape at 20 kV accelerating voltage for 120 s count time; the analytical data were obtained using INCA software.

Finally, cold cathodoluminescence (CL) microscopy was applied for unveiling further compositional details of the mineral grains at LMRR, using a Leitz Wetzlar Orthoplan Microscope on which a Reliotron III cathodoluminescence system is attached. The conditions used were 10 kV excitation voltage and 0.200–0.400 mA current. Images were captured with a canon powershot A630 digital camera.

3. Results

3.1. Mineralogical, chemical and structural analyses

3.3.1. Optical microscopy

Sample DC-LIR1 was thin sectioned to be examined under a polarizing petrographic microscope (PLM) equipped with a progress Jenoptik digital camera aiming to characterize it both compositionally and texturally. Fig. 7a and b indicate that sub-angular to sub-rounded quartz grains predominate (>95% per volume), whereas potassium feldspar, quartzite fragments and argillite fragments are only rarely encountered. The size of the grains ranges from 0.2 to 0.6 mm (medium to coarse sand) with rare exceptions up to 0.8 mm (maximum grain size = 0.85 mm). All grains are consolidated together through a cementing material which is either of siliceous composition (up to a depth of 4 mm from the upper reddish colored external surface; see Fig. 2) or iron rich siliceous (at depth greater than 4 mm from the upper reddish colored external surface; see Fig. 2). In the former case the thickness of the cementing material can reach up to 9 μm, as Fig. 7c and d indicate, whereas in the latter case, it never exceeds 4 μm (Fig. 7e and f). Fig. 6 presents the sample and the axis of sampling.

Following a very careful examination of the quartz grains, their detrital origin can be recognized. Their shape is rounded to subrounded, but it is always severely obscured by the development of authigenic quartz over their rounded borders. Occasionally, the rounded shape of the detrital grains is nicely outlined due to their abundant tiny inclusions they contain, which however are completely lacking from the authigenic overgrowths (Fig. 7c to f). The abundance of such inclusions coupled with the undulatory extinction observed in most of the detrital quartz grains indicate their genetic affinity to metamorphic parent rocks. The grains are homogeneously distributed and are very well sorted. The

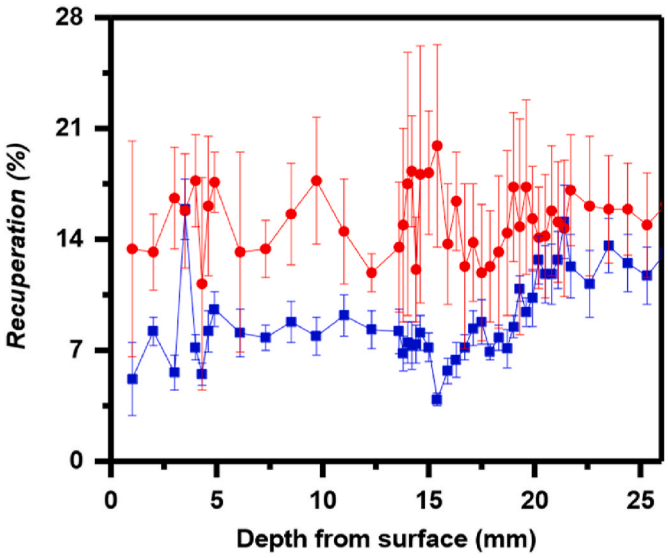

Fig. 5. Recuperation values versus depth from the surface for both samples (red dots for the bleached and blue squares for the original). Each data point corresponds to an average over two individual measurements for the same layer. For the sample that has been subjected to bleaching, the recuperation values are by two-fold increased, indicating the effect of intense charge transfer.

petrographic analysis conducted has verified the sedimentary character of the analyzed rock, which due to the dominance of monocrystalline quartz grains can be classified is a typical quartz sandstone which due to the great amount of quartz can be referred to as quartz arenite (Fig. 7a and b). Compared to an earlier studied cobble the present sample is significantly more mature and coarser (medium to coarse sand) than the very fine to fine sand sample analyzed previously in Liritzis et al. (2019). Indeed, the intergranular pore space is considerably less represented in sample DC-3 (Fig. 7 e,f) compared to the counterpart reported in Liritzis et al. (2019). Similar differences can be outlined in terms of the chemical composition of the two samples (see, Table 3). Sample DC-3 is the one more siliceous (97% wt in respect to 94.1% wt if the less iron-rich parts of both samples are considered).

On the other hand, if the Fe-rich parts of the two samples are considered then sample DC-3 contains higher amounts of Al_2O_3 (19.97% wt in respect to 4.21% wt) but is significantly poorer in Fe content (1.67% wt in respect to 60.90% wt). Then the larger size of DC-LIR1 sandstone and sampled grain sizes coupled with Fe-stained coated grains, patina and weathered status, action of seepage of water into the samples and the cracking in that studied rock piece and the diffusion of weathered solution, produced a complex dose and dose rate evaluation consequence and consequently the age estimates. These differences in mineralogy and different origin of stone that fell from flaking, strengthens further the chronological significance of the obtained dates in this ongoing project in Indian Daraki-Chattan cave and associated rock art.

3.1.2. Cathodoluminescence

Cathodoluminescence analysis was performed to get an idea of the structural status within the piece overgrowths on detritus quartz implying possible chemical and/or physical changes during growth. The specific analysis was performed on a non-polished, uncovered thin section prepared from the original specimen. The thin section was examined under the cathodoluminescence microscope across its length as the red arrow indicates. Images of Fig. 8 were captured with a Canon Powershot A630 digital camera. According to this image, the thin section across the sample exhibit differences between luminescence of quartz grains (Fig. 8). Specifically, blue- and dull cyan-luminescent quartz crystals were identified. Such discrepancies offer a first insight

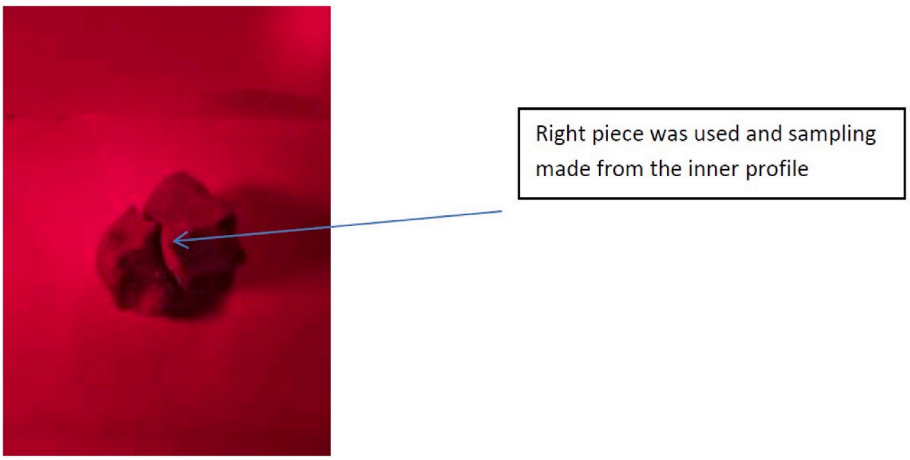

Fig. 6. Sampling of the clast in red dim light conditions, upper surface was exposed to sun light in Rhodes Island, Greece.

into the depositional processes of the sample under examination.

Blue-luminescent quartz is attributed to the detrital origin of such grains, whereas dull cyan to red-luminescent quartz indicates their possibly authigenic origin. It is worth noting that in many instances (indicated with red arrows in Fig. 8) quartz grains exhibit a sub-rounded shape under CL observation, which is however heavily obscured through transmitted light observation. In fact, under plane polarized light the same grains appear angular to subangular due to their overgrowth by authigenic quartz, which is only revealed during the CL evaluation. In fact, petrographically it is quite far from what we call metamorphic quartzite. In a metamorphic quartzite we have recrystallization of quartz, therefore we would not expect the evidence to be evident regarding its authigenic or detrital origin and which are recognized by cathodoluminescence but also by careful petrographic observation. It is thus a sandstone that has undergone a high degree of diagenesis and the studied sample a quartz-arenite.

3.1.3. X-ray powder diffraction analysis

Fig. 9 presents typical X-ray diffractograms that were acquired for a selection of sample layers. Mineral identification was feasible by the interpretation of these, based on the International Centre for Diffraction Data Powder Diffraction File (2006). Quartz (Qz; SiO_2) was revealed as the main mineralogical phase; nevertheless, traces of birnessite (Br; $Na_{0.55}Mn_2O_4{\cdot}1.5H_2O$) and afghanite (Af; $(Na,Ca,K)_8(Si,Al)_{12}O_{24}(SO_4, Cl)_3$) could be also detected throughout the depth of the sample.

3.1.4. Bulk chemical analysis (XRF/EDS)

The mean of five runs of the XRF/EDS analysis of the whitish part of the sample and the mean of three runs of the reddish part are given in Table 3. The major elements content of the sample DC-LIR1 reported by Liritzis et al. (2019) is also given for comparison reasons. Table 3 presents the SEM-EDS data on specific points of the profile for minerals and chemical elements corresponding to Fig. 10. It is worth noting the presence of zircon which implies high dose in that area and respectively may explain the individual high doses in some rare occasions along the profile.

3.4. OSL analysis and dating

3.2.1. ED profile description

Fig. 11 presents the depth profiles of both natural equivalent doses for the buried clast (curve a) and the equivalent doses of the bleached analogue (curve b). At the same figure, the boundaries within the collected samples are also presented. The term “boundaries” is used, as these indicate areas where physical properties of the sample, such as texture and color, change; the major sub-sectioning of the samples due to different physical properties is tabulated in Table 1. As it becomes quite prominent from this latter figure, the behavior of the ED indicates a number of intense spikes, namely not continuous and quite steep intensity discontinuities. These could be attributed to the main usual concerns with the current OSL SLD technique, such as uncertainties due to coring, slicing and labor-intensive sample handling in general, because of frequent mechanical breakage, leading to uncertainties in depth estimates, random inter-slice scatter in OSL intensity and spatial resolution problems.

It is quite interesting to note that both macroscopical observations as well as analytical measurements using XRF, XRD, SEM-EDS and PLM indicated that the presence of spikes is monitored within the depths that are correlated with associated change of the physical properties within the sub-pieces. For the outer soft and reddish-brown material, the grains were coated with reddish (Fe, Mn)-aluminosilicate which occurred in situ, i.e. is post-depositional. The weathered solution covers grains along their cracked path resulting to a cemented coating of appreciable thickness which obviates luminescence light and their radiation emission to be detected (Liritzis et al., 2019). Effects of both staining and coating to quartz grains because of iron have been observed via SEM-EDS and stand as the main reason for the lack of totally zeroed quartz grains in the outer surfaces of either sub-piece. Similar to our previous study on the same archaeological site (Liritzis et al., 2019), the ED of the outer surface layer that has been exposed to light for prolonged time is not zero. Instead, a residual level of ED value was calculated which is explained as rather charge transfer process (see, also Liritzis et al., 2008). For the piece which is soft at the outer part regarding some high dose spikes in the surficial layers especially, it can be explained due to diffusion into the quartzite for (a) variable sunlight bleach and (b) intrusion of potassium hydrolysates. The potassium values are variable and problematic as observed here (see Table 5), and the 0.03 (inner core) versus 0.4 (outer layers) of K_2O values in the present piece of rock is indicative. For the latter, the presence of anomalies in the concentration of some elements (in metals, such as K, Na, Mn, Mg, Ca and Fe, and in non-metals, such as, F and P) can be related to possible contamination because of elements fixation (Brinkiene et al., 2016). Compounds of sodium and potassium are abundant in nature and highly soluble in water. Some groundwater contains moderate amounts of dissolved material and transport of K^+ (and rubidium, a beta emitter too) will be controlled by diffusion into bed sediments and harder media e.g. rocks (Du et al., 2005) as predicted and observed transport concentrations of K has been documented (Jackman et al., 1984).

3.2.2. Physical interpretation and assessment of the ED profiles

Concerning the Equivalent dose (ED) profile versus depth, the spikes that are associated with quite large ED values imply domination of a

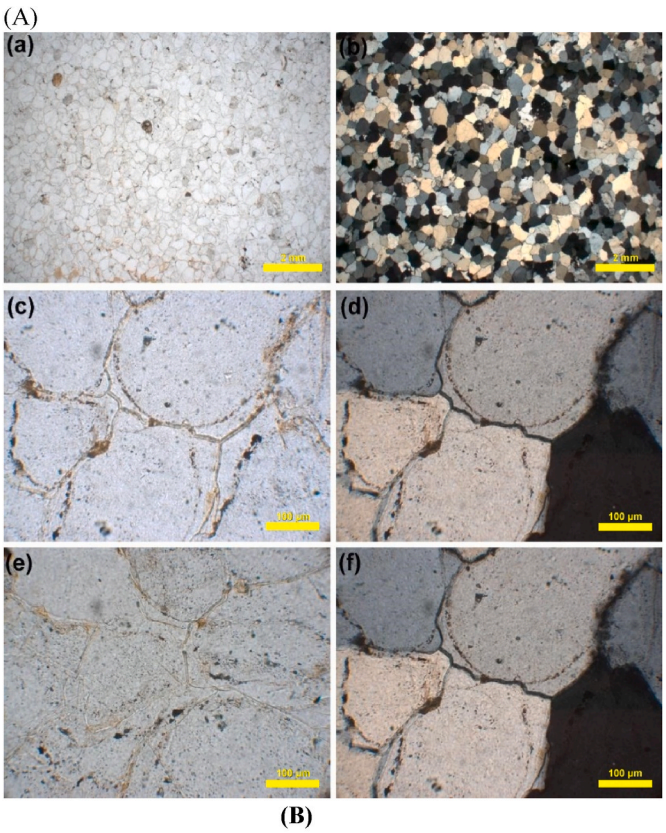

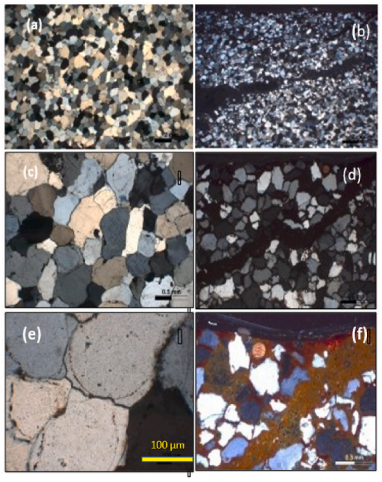

Fig. 7. **(A)** Representative photomicrographs of sample DC-3 considered in the present study, examined under a polarizing petrographic microscope (PLM). The presence of such inclusions, together with the undulatory extinction found in the majority of the detrital quartz grains, suggests that they are genetically related to metamorphic parent rocks and size of the grains ranges from to 0.20–0.85 μm. a) and b) predominant sub-angular to sub-rounded quartz grains whereas other minerals are only rarely encountered; c) and d) grains consolidated through a cementing material of siliceous composition reaching a thickness up to 9 μm; e) and f) cementing material of iron rich siliceous, whereas thickness never exceeds 4 μm. **(B)** Representative photomicrographs of sample DAR3 (left column) compared to those reported for the sample analyzed (right) in Liritzis et al. (2019) for DC-1.

Table 3
The fresh surface of the buried sample analyzed by means of XRF/EDS. The average over five individual measurements of the XRF/EDS analysis of the whitish part of the sample and the mean of three runs of the reddish part. Comparison with earlier sample DC-1 (or DC-LIR-1 in earlier publication).

	DAR3 whitish part	DAR3 reddish part	DC1 whitish part	DC1 reddish part
MAJOR ELEMENTS (oxides in % wt.)				
SiO_2	97.00	82.13	94.10	20.61
TiO_2	0.02	0.23	0.08	0.42
Al_2O_3	2.12	13.97	4.94	4.22
Fe_2O_3	0.11	1.67	0.46	60.90
MgO	0.08	0.48	–	0.33
MnO	ND	0.03	–	1.30
CaO	0.07	0.12	0.13	0.06
P_2O_5	ND	0.14	–	–
K_2O	0.03	0.40	0.05	0.24
Na_2O	0.13	0.26		–
TRACE ELEMENTS (ppm)				
V	10	78		
Cr	6	42		
Co	6	5		
Ni	4	20		
Cu	99	19		
Zn	6	14		
Rb	ND	6		
Sr	16	15		
Y	4	5		
Sn	93	75		
Ba	65	79		
Hf	ND	10		
W	ND	17		
Pb	3	13		

sensitive fluorescent mineral (mostly quartz and in some cases feldspars), a feature that was easily revealed by the PLM measurements. In contrast, low ED values imply the presence of faint, or even non-luminescent minerals (such as mica or iron oxides) and/or absorption from an attached to grains non-luminescent medium; the former feature was also verified by the corresponding PLM measurements. This varied spatial luminescence response and its effect on the luminescence-depth profiles is an important find.

Signal or ED depth profile stands as the most important feature of rock SLD, as it enables the identification and, under certain circumstances, the dating of multiple burial and exposure events. Both dose profiles of the present study increase towards a seemingly saturating exponential value. Nevertheless, the presence of spikes makes the interpretation of these profiles quite difficult. Thus, several data points were treated as outliers and were rejected following physical/mineralogical criteria imposed by the characterization techniques applied (compare Figs. 11 and 12). Fig. 12 presents the corrected equivalent dose depth profiles for both bleached analogue as well as the original quartzite, following rejection of the outliers; both profiles are presented in the same plot for the sake of comparison. The few data points of the ED profiles were considered as outliers and thus rejected, and the rejection reason was a combination of (a) ED value that is not following the expected S-shaped pattern along with (b) CL and PL measurements that indicated very faint or very bright points and (c) compositional data that provide solid proof that at these specific points, there are spatial phase transitions.

Both profiles indicate the same behavior up to the depth of ~13.5 mm, yielding the typical S-shape that is attributed to the attenuation of daylight flux causing differential eviction of trapped charges with depth. A plateau (P1) is observed between ~ 6.5 and 15 mm of depth, displaying a flat ED distribution (with some scatter). Such a plateau is expected to form during burial by uniform dosing of a previously bleached rock profile. In deeper sampling the onset of saturation is reached. This is applied for a fresh rock surface which is for the first time exposed to light, which then penetrates the surface; the higher the

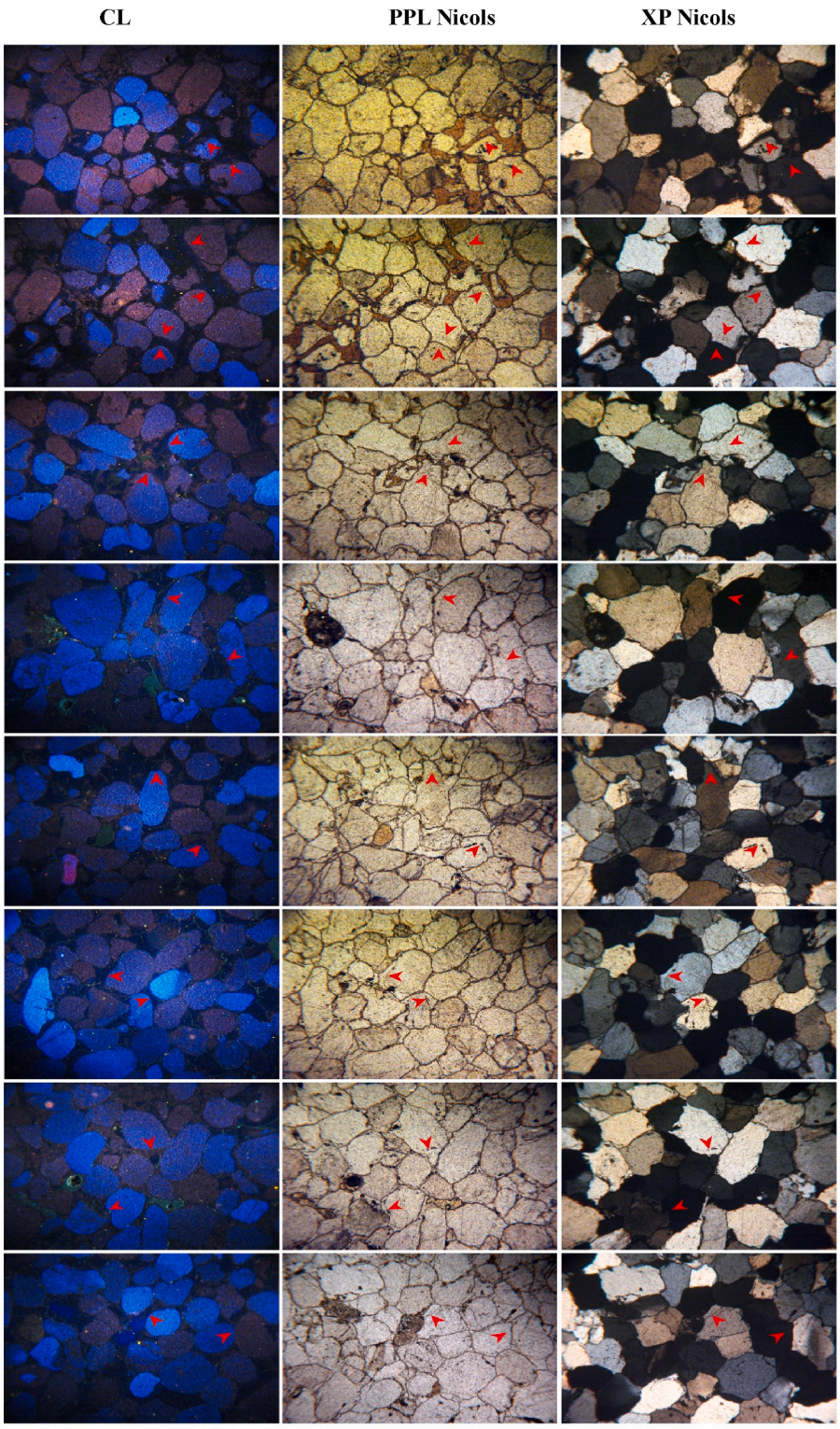

Fig. 8. Representative photomicrographs along the thin section profile (red vertical arrow of Fig. 10a) acquired using the cathodoluminescence apparatus (left column) and their relative view under transmitted light (center column: PPL = plane polarized light; right column: XP = crossed Nicols). In several occasions indicated with red arrows, the quartz grains display a sub-rounded shape under CL observation, severely obscured through transmitted light observation.

exposure time the more activation energy is reaching the traps and more electrons are released, that is, more OSL light is measured. Thus, during exposure, the traps in layers near the surface are first emptied, and those in the deeper layers follow an exponential-like function of having been bleached, until the saturation is reached. It becomes prominent that the common equivalent dose profile saturates at around (55 ± 5 Gy). This latter value was calculated via a fitting approach according to the following equation by Polykreti et al. (2002):

$$\mathrm{ED}(x) = \mathrm{ED}_{\mathrm{res}} + ED_{sat} \bullet e^{-\mu t \cdot e^{-kx}}$$

It is worth mentioning that the former equation was not applied for the calculation of the bleaching duration-age of the quartzite clast

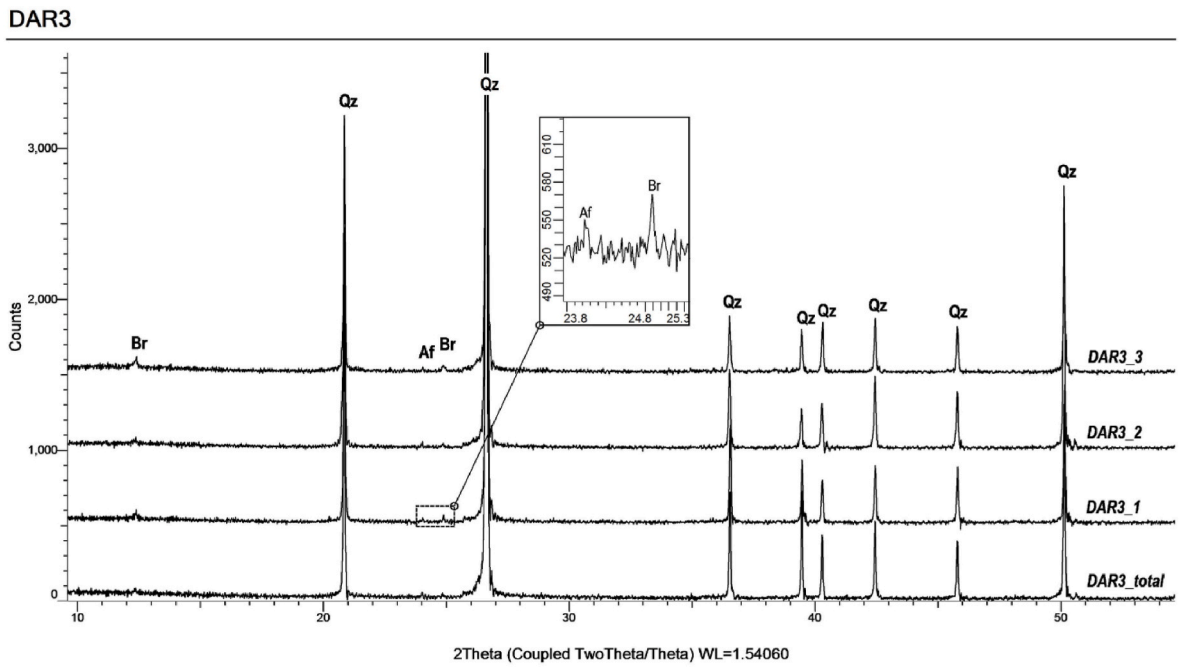

Fig. 9. The XRPD patterns obtained through the analysis of the whole rock for DAR3-1, 2, 3 points of Fig. 3b.

sample. This was not possible as many parameters of the aforementioned equation are unknown. This equation was used in order to estimate the saturation level ED_{sat} (55 ± 5 Gy), the light attenuation coefficient k (0.595 ± 0.063 mm^{-1}) and, indirectly, the bleaching front, namely the depth at which the ED gets the 50% value of the corresponding saturation value of 55 Gy. The bleaching front was calculated at ~ (2.4 ± 0.1 mm) and it is indicated as a vertical line in Fig. 12. As expected, in the first ca 2.5 mm from top the ED of the bleached experiment are lower than the buried rock sample. These results indicate that the ED plateau is enough wide, ranging between ~7 and 13.5 mm, corresponding to a prolonged exposure time.

These are the common features of the two ED profiles. In contrast, beyond the outer 13.5 mm, these profiles show prominent differences. In fact, the corrected dose profile for the buried rock art yields the presence of another plateau P_2. The increase of dose beyond a first wide plateau slowly reaches another flat area, which however is not so prominent due to scattering, saturating at (85 ± 6 Gy). In general, the features of this second single-plateau profile were also revealed following fitting using the previous equation. Typical values for the light attenuation coefficient k is (0.463 ± 0.051 mm^{-1}) and the bleaching front of the P2 is (17.3 ± 0.3 mm) from surface. Finally, this plateau is also quite wide, ranging between ~21.5 mm up to the last measurement, at around 28 mm.

For the bleached analogue, beyond 13.5 mm the ED profile indicates a step-like increase of the ED that is followed by another plateau P_3, as much wide as the first one, saturating at ~ (65 ± 5 Gy) (see Fig. 12). As this step-like increase takes place within only 3–4 data points, fitting and calculation of either light attenuation coefficient k or bleaching front becomes physically meaningless. This second plateau is monitored up to a depth of 23 mm; deeper, the ED value starts decreasing monotonically for depths up to ~27 mm.

The shape of both equivalent dose profiles, consisting of two dose plateaus, provides a strong hint towards a multiple exposure event in the history of the sample. These events could be either irradiation events, corresponding to a stability level of the ED, or exposures to sun light. The equivalent dose profiles of Fig. 12 resemble the corresponding curve $L_4(x)$ of Freiesleben et al. (2015, their Fig. 1), of Liritzis et al. (2019, their Fig. 4) and Liritzis et al. (2017, their Fig. 4). The physics of trapping and de-trapping of electrons during radiation and light exposure along with the gradual bleaching of luminescence quantified as a function of depth which produces a family of sigmoid-like saturating exponential curves shifted with depth corresponding to certain sun exposure times, have already been discussed in Liritzis et al. (2017).

When a piece of the petroglyph detaches and falls and is buried to the ground, being covered with surrounded sediment, the bleached electron traps of the first millimeters from surface *are filled* with electrons due to the irradiation of the grains from environmental gamma rays and the alpha and beta particles of the rock piece itself, *continuously up* to the day of measurement in the laboratory. The increase of dose in these emptied traps when it was exfoliated is sensible with respect to the higher levels in deeper layers. At any rate, the second onset of plateau cannot be defined whether it corresponds to a second exposure time (or first exfoliation) or it is the rock's geological saturation level. As we are not aware if there was another detached part from the present piece of clast, we may consider a possible first event (possibly exfoliation or burial event) which resulted to the accumulation of the 85 ± 6 Gy and a second burial event for the first plateau of (55 ± 5 Gy). Therefore, the two equivalent doses can be used for definitely one, but possibly two, burial ages. Nevertheless, there is also the possibility that the plateau ED value of (85 ± 6 Gy) corresponds to the equivalent dose accumulated since the production of the rock art. Following the above rationale, however, in the present study the first plateau suggests one exfoliation event accumulated the equivalent dose value of the P_1=(55 ± 5 Gy). Finally, a residual dose of 4.90 ± 0.37 Gy is obtained for the first surface layer measurement which implies either a recent exposure or most probable faint/non-luminescent minerals as explained above through PPL and CL.

Moreover, according to the dose depth profile and the abrupt change monitored for the lower face of the rock art sample, it is concluded that this lower face must have been the outer face detached from the rock. In contrast, the exposure to the sun was performed to the inner detached face of the rock; the gradual reduction of dose versus depth in the lower part of the profile that sampling commenced was the one exposed to daylight. Unfortunately, since the material was very soft at the inner part, sampling and measurements of the final layers deeper than 28–29 mm was not possible.

3.2.3. Dose rate

The present U, Th measured values are similar to the earlier sample

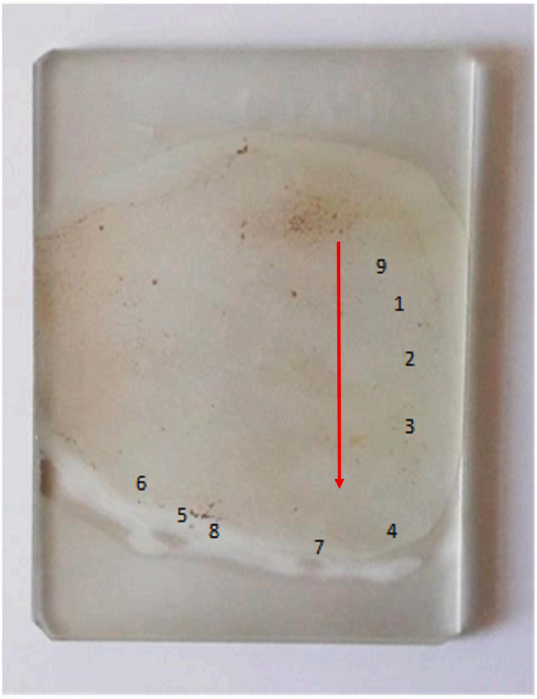

(A)

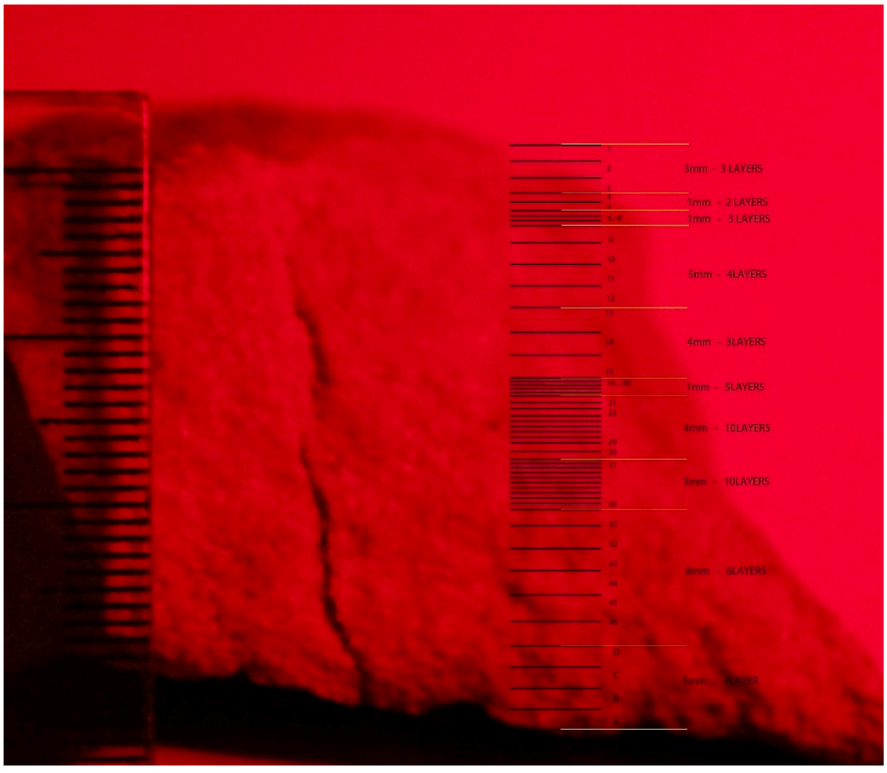

(B)

Fig. 10. A: The profile with numbered points analyzed by SEM-EDS data on specific points of the profile for minerals and chemical elements in Table 4. The red arrow indicates the sequence through which the photomicrographs acquired with the CL microscope. **B:** respective depth in mm (red) magnified to read the layers' numbers and thicknesses of DC-3 (see Table 4).

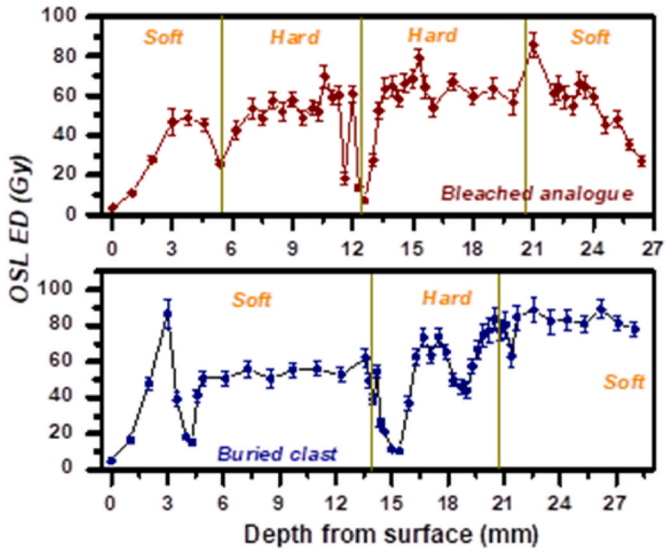

Fig. 11. Equivalent dose (ED) profile versus the depth from the surface for the original clast sample coming from the rock surface above the ground (lower plot) as well as the bleached analogue (upper plot). In both profiles, spikes and discontinuities are obvious and could be attributed to the phase/composition discontinuities of the sample core. In general, both profiles provide trends for the presence of at least one plateau, along with a final saturation plateau at the edge of the core. Vertical lines present boundaries for areas indicating similar mechanical and optical properties; analytical techniques suggest also similar composition.

DC-1, with U = 0.70 ppm and Th = 3 ppm which are low, compared to other measurements in literature for sandstones: 4–7 ppm for Th (on average 5.5 ± 2 ppm), and 1–2 ppm for U (on average 1.7 ± 0.7 ppm); while for sand-sized quartz Th concentration is 3 ppm and that of U is 1 ppm. Other minerals deposited in hydraulic equilibrium have on average Th = 4 ppm and U = 1 ppm (see, Rogers and Richardson, 1964). Sandstone and conglomerate are sedimentary products of weathering, erosion, deposition and cementation, similar to shale. Unlike shale, they seldom have a high content of radioactive minerals when deposited. However, they are much more porous and permeable and often host U and Th minerals deposited by groundwater. This latter case occurs in the present sandstone exfoliated from the rock art facade.

Obviously, during exfoliation it fell on the ground and gradually became buried into the sediments by percolating waters and sediment development from various sources. This gives a variable gamma dose rate over time. Today the gamma ray dose-rate is considered over 4π geometry, giving full dose to the sample. The actual value of gamma dose rate should be lower. At any rate this uncertainty falls within the uncertainty of the calculated gamma dose rate. Water uptake (in the cave entrance stratigraphic profile, see Fig. 1) is estimated to (50 ± 20)% throughout the years applied to the sediment not the rock sample. In fact the cave is moderately dark in its deeper part, as the large vestibule permits ample light to enter. The light has not been measured. The cave is completely dry most of the year, but during monsoons, there might be water on the walls. The large sandstone clasts dominated gravel 70% and sand 10% and only ~20% clay and weathered limestone deposit, giving an uncertainty only to the gamma rays from the context.

Considering all above factors, the dose rate derived from the U, Th, K, Rb of the rock itself and the surrounding sediment (mainly clasts), consists of respective alpha particles dose rate (from U, Th) of the stone piece, beta particles dose rate (from U, Th, K, Rb) from the stone piece, gamma rays dose rate (from U, Th, K) from the context and cosmic rays, and an assumed 0.1 Gy/ka internal dose for the quartz grains. It is equal to 1.20 Gy/ka. More details are tabulated in Table 5.

3.2.4. *Age estimation*

The sample after an unknown time on the rock surface had been subjected to sun exposure with total bleaching to zero from surface into the inner part of the rock to several mm, followed the time from when this rock piece became buried in the sediment. Upon burial, these zero parts filled with a constant added dose which makes the first millimeter layers enhanced in dose up to an initial flat region. This occurs between 6 and 13 mm.

The total dose accumulated during burial in this range is P_1=(55 ± 5 Gy). The deeper parts are partially bleached to finally reach an apparent saturation level which is either a second burial or indeed the geological luminescence. Thus, between 21.5 and 27 mm the gradual increase reaches the saturation at the P_2~85 Gy. Then at the first layers like a residual dose implies exposure as reported earlier.

From the above petrographic and luminescence data and considering various events in the history of the exfoliated and buried piece to be dated, we calculate the following ages in years before current era (BCE):

Age = ED P_2/DR or *71 ka* ago *(±12%)* and the second burial age is:

Age = ED P_1/ DR or 46 *ka* ago (± 10%).

From an earlier dating project from the same cave and rock art an exfoliated piece bearing cupule of around 13 ka BCE broadly coincides to the end of the last glaciation, demise of the last ice (Late Glacial and Younger Dryas) and transition to the milder climate of the Holocene (Liritzis et al., 2019). The low ED at the beginning around 4 mm from surface cannot be explained at present attributed to a more recent burial event (~4 ka ago) or most probable faint/non-luminescent minerals as

Table 4
The profile with numbered points analyzed and minerals.

Various mineral phases				Cement matrix (Average over 5 independent measurements)				
Sample	**DC-3**	**DC-3**	**DC-3**	**Sample**	**DC-3**	**DC-3**	**DC-3**	**DC-3**
analysis	pic3	pic4-1	pic4-3	analysis	pic1	pic4	pic5-6	pic9
mineral	?	baryte	zircon					
SiO_2	–	–	32.56	SiO_2	57.95	56.90	37.05	63.51
TiO_2	–	–	–	TiO_2	–	–	1.34	–
Al_2O_3	33.59	–	–	Al_2O_3	39.19	43.10	30.68	23.78
P_2O_5	31.64	–	–	P_2O_5	–	–	2.97	–
Cr_2O_3	–	–	–	K_2O	–	–	0.62	3.05
Fe_2O_3	–	–	–	Fe_2O_3	2.86	–	27.34	8.84
MgO	–	–	–	MgO	–	–	–	0.82
CaO	1.45	–	–	CaO	–	–	–	–
SrO	7.49		–	Total	100.00	100.00	100.00	100.00
BaO	–	59.71	–					
SO_3	3.37	40.29	–					
La_2O_3	3.99		–					
Ce_2O3	7.23		–					
ZrO_2	–	–	67.53					
Total	88.76	100.00	100.09					

Table 5
Radioisotopic content of U, Th, K for rock and surrounding (sur-reddish), the dose rates of alpha (D_a), beta (D_β) and gamma ray (D_γ), total doses and ages before current era (BCE). Dose rate conversion factors are from Liritzis et al. (2013b).

U ppm[a] rock/sur	Th ppm rock/sur	K_2O%[b] rock/sur-red	D_a[c] Gy/ka	D_β Gy/ka	D_γ[d] Gy/ka	D_c, Gy/ka	D_q[e] Gy/ka	Dose Rate[f] Gy/ka	D, Gy	Age, ka BP
0.70/2.60 (±0.075, 0.25)	3.00/10.60 (±0.3, 1.0)	0.03/0.4 (±0.003, 0.04)	0.16 ± 0.018	0.13 ± 0.011	0.56 ± 0.04	0.25 ± 0.05	0.1 ± 0.01	1.20 ± 0.13	55 ± 5 85 ± 6 (4.9 ± 0.4)[g]	46 ± 4 71 ± 5 (~4.1)

[a] The K, U, Th were also measured using a portable NaI scintillometer as average over three readings (K = 0.4 ppm, U = 2.6 ± 0.3 ppm, Th = 10.6 ± 0.3 ppm) made by Robert Bednarik for the excavators. Similar values we obtained from SEM-EDS. In fact, colleagues from Ahmedabad NRL India (A. Singhvi et al.) comment that there is a problem with K value. It is used to seeing numbers like 1% but since the low (ppm) value is given in numbers by the NaI (Tl) from R. Roberts (Australia), they used the same value (Pers comm. 27 February 2016 to Giriraj Kumar from Ashok Singhvi). The rock's U and Th was measured by calibrated alpha counting. At any rate aluminosilicates when subjected to the hydrolysis reaction produce a secondary mineral rather than simply releasing cations, thus leaching potassium e.g. $2KAlSi_3O_8 + 2H_2CO_3 + 9H_2O \leftrightarrow Al_2Si_2O_5(OH)_4 + 4H_4SiO_4 + 2\,K + 2HCO_3$.

[b] Potassium oxide K2O measured by SEM-EDS equals 0.03% and 0.40% for the white and external reddish colour respectively. Potassium% = K2O*0.83013. Rb is taken as K/Rb = 200, Rb=K/200 = 0.1/200 = ~0.0005 = 0.

[c] Today the gamma ray dose-rate is calculated over 4π geometry, giving full dose to the sample. The actual value of gamma dose rate should be lower. At any rate this uncertainty falls within the error bars of the calculated gamma dose rate.

[d] Water uptake is taken 50% and applies to environmental radiation not to the D_α and D_β of the rock itself. $D_{\gamma,wet} = D_{\gamma,dry}/\{[1.14\,(w/d-1)] + 1\} = D_{\gamma,dry}/1.57$, w = saturated weight, d = dry weight.

[e] Internal dose-rate to quartz.

[f] The corrections to D_α, D_β, D_γ dose rates are given in the text, Section 4.7.3.

[g] The age implies a possible exposure due to re-arrangement of strata.

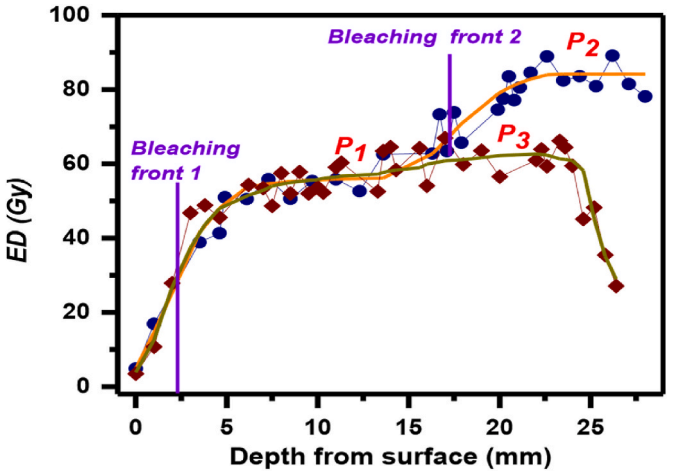

Fig. 12. Equivalent dose (ED) profile versus depth from the surface for both the bleached analogue as well as the original sandstone (quartzite) clast sample; in both profiles some data points yielding spikes and discontinuities were removed as outliers. Lines correspond to the best fit profiles according to equation of Polykreti et al. (2002) for various bleaching and irradiation events. Vertical lines correspond to the bleaching fronts corresponding to the two main plateaus. Brown diamonds represent the bleached experiments and the blue solid circles data of original rock profile. The two equivalent doses of P1 and P2 imply definitely one but possibly two burial ages or the P2 refers to an exfoliation or burial event and the P1 another burial event. It is possible that the P2 plateau corresponds to the equivalent dose accumulated since the production of the rock art. P3 plateau is monitored for the bleached analogue sample.

explained above (Table 5).

4. Discussion

As Fig. 11 reveals, the majority of the OSL ED spikes occur very close to the boundaries, as these were identified by the complementary analytical characterization techniques, providing thus strong evidence regarding the uncertainties due to mineralogical heterogeneity and presence of phase transitions-alterations within the host material (McKeever, 1985; Townsend et al., 2002, 2008). Besides dosimetry and dating, several alternatives and, at first sight, unlikely applications have either been reported or just attempted using luminescence, mostly in terms of TL. A full list of these applications would, undoubtedly, include solid-state crystal and defect structure analysis (McKeever, 1985). Luminescence efficiency, emission spectra, and excited state lifetimes (and thus ED as well) are all influenced by a number of factors, the most common of which being the crystalline phase, pressure and temperature (Townsend et al., 2008; Polymeris et al., 2017). Discontinuous changes in these luminescence parameters occur during phase transitions whilst exciting, heating, or cooling, the samples. Phase changes also occur due to impurities and adsorbates attributed to moisture, as these modify the host material reflect on crystal growth and surface treatments. The changes of the luminescence intensity/sensitivity imposed by ionizing radiation to the physical properties of various minerals are at the same time numerous as well as extremely rapid. In other words, OSL ED fulfills the requirement for high sensitivity and discrimination associated with identifying the presence and behavior of both host and precipitate phase transitions (Polymeris et al., 2012, 2017). Luminescence offers detection of phase inclusions or surface defects even below the ppb levels (McKeever, 1985; Townsend et al., 2002, 2008), yielding detection thresholds comparable, or slightly worse than the 10^9 - 10^{10} spins for the case of Electron Paramagnetic Resonance (EPR, Ikeya, 1993).

The sample DC-3 considered in this report is classified as a quartz arenite. The petrographic characteristics of this rock highlight its high textural and mineralogical maturity, composed mainly of monocrystalline quartz of medium to coarse sand size and only traces of polycrystalline quartz (quartzite) and argillite fragments. Concerning the non-luminescence in three depths for buried and modern bleached ones (~4–5, 11.5–13, ~15, ~21 mm) the cathodoluminescence spectra give some clue, by giving dark areas of non-luminescence, yet the SEM-EDS taken in three points (Table 3) did not result in any unusual presence of non-luminescent oxides but implication for non-luminescent induced radiation is possible (Pinnioja, 1998). The latter has been observed and OSL and TL intensity is influenced by impurities in the mineral lattice, such as aluminium, iron, germanium and copper atoms (Schmidt et al., 1974; McKeever, 1984, 1985; Poolton et al., 1996). Al and Fe have been readily found in the analysis of the DC-3 quartzitic sandstone. A model proposed by Hashimoto et al. (1997), which analyses the role of Al impurity in the lattice, explains the role of the luminescence based on observations made in electron spin resonance (ESR), nuclear magnetic resonance (NMR) and neutron activation analyses (NAA). In the case of small Al impurity concentrations, about 30 ppm, a relatively large number of Al-hole centers will be created. These centers act as

luminescence centers at the blue band of the spectrum (Hashimoto et al., 1996). *Low* Al impurity concentrations in minerals are formed during slow cooling of magma - such as in plutonic rock formation. Higher impurity concentrations, above several tens of ppm, are accompanied by high concentrations of hydroxyl (OH-) bond, possibly caused by crystals formed during fast cooling of magma as in the case of extrusive (volcanic) rock formation. During irradiation, the hydroxyl sites will induce the formation of H° atoms, which because of their small size are labile and mobile within the quartz lattice. As a result, the H° atoms readily combine with the Al-hole centers, and the radiation-induced signals from surrounding radiation sources (U, Th, K, Rb, Cosmic) disappear (McKeever, 1985; Hashimoto et al., 1996, 1997). These holes, or "killer" centers emit radiation outside the detected wavelength band.

The variations of dose in the bleached luminescence from the top surface to the inner parts of the rock follow a similar increased dose towards a saturating exponential as the original surface. The similar behavior of doses implies that the nine months of sun exposure has not resulted in sufficient bleaching below the surface but the anticipated lower residual at the first about 3–4 mm below the top. The traps at deeper layers follow an exponential-like function of having been bleached via a double exponential fitting (Polykreti et al., 2002), yet it has been shown that an error function of cumulative log-normal distribution equation, for ancient marbles and granites, with attaching physical meaning to coefficients, can produce family curves as a function of exposure time (that is the age) and a shift of the saturation exponential curve to higher depths (Laskaris and Liritzis, 2011). This latter approach is under further investigation.

The accumulated luminescence dose since burial defines the time the stone has fallen providing a constrained terminus *post quem* for the carved adjacent petroglyphs the earliest being ~71 Ka ago. Hence, concerning the magnitude of the age of the deposition of the clast it is slightly postdating an exfoliated cupule fragment: it does not date the rock art, which is already known to be of Lower Palaeolithic antiquity. Thus, it provides a very conservative minimum age, because we cannot estimate how long it took to exfoliate from the cave wall.

To recapitulate, (a) the complex combination of present multiple petrographic characterization of mineral grains along the piece of stone profile, coupled with dose profiles, and (b) the due care in taking luminescence readings, in conjunction to (c) respective theoretical interpretation of dose and dose rate and age results, form a robust methodology which strengthens our study.

The limitation of our methodology lies in the constraint chronology of stone fall. Another point needing attention concerns the meticulous sampling along a piece of rock and its facing surface when in the rock and which is detached from the rock. Such restrictions in attributing reliable dose plateau and hence find exposure-burial histories can be tested with a modern sun exposure of the same rock for a period of some weeks or months as we have done and compared with the original profile. Last, some low or non-luminescent minerals (confirmed and by CL) do not follow the expected trend of dose versus depth and are removed.

5. Conclusions

The Indian rock art site Daraki-Chattan is the subject of an ongoing project regarding chronological appraisal of famous petroglyphs in situ and those exfoliated found deep in the site's sediment. OSL and various petrographic analysis were combined to provide an objective age determination of a sedimentation event postdating the deposition of an exfoliated slab bearing cupule, which has been achieved with a detailed supportive methodological approach. The quartzite clast piece DC-3 was found buried in under 2 m of very coarse sediment as can be seen from the images (Fig. 1b and 2), and the accumulated luminescence dose since it became concealed provides a conservative minimum age for the rock art found stratigraphically below it. The time span elapsed between the time the cupule was created on the cave wall, became exfoliated, transported by gravity through the cave entrance, then covered by sediment needs to be added to the burial time of DC-3 to estimate the age of the rock art. That time span remains entirely unknown. But two burial-sun exposure events are recorded at around 46 ka and 71 ka ago. Analytical investigation of the mineralogy of the sampled profile of this piece of rock with detailed microphotography, SEM, CL, XRD, XRF, explained the dose behavior in particular depths from the top of the rock piece.

The studied rock sample is estimated to have been buried about 46 ka ago and represents a last burial event with another possible exposure-burial event of same clast occurring at around 71 ka ago. These burial events provide a most conservative *terminus post quem* for the petroglyph found below it, which was probably made during the site's Oldowan Mode 1 occupation.

The presented methodology provides novel OSL chronological information from a challenging archaeological setting where few other dating approaches would succeed. Also, it contributes to understanding the complex signal-depth profiles in rocks; this is important since the signal resetting with depth is a unique tool only available with rock surface dating. The combined OSL dating of the fallen exfoliated rock piece with petrographic analysis, shows that those analytical tools are complementary to each other and support the proper manner to assess radiation dose rates and equivalent luminescence dose. Beyond weathering status of rocks, the presence of non-luminescent minerals along the present rock equivalent dose profile is also dealt with properly.

Author contributions

"Conceptualization; I.L.; R.B.; G.K.; methodology; I.L.; G.S.P.; I.I.; V.X.; software; I.L.; R.B.; G.K.; G.S.P.; validation; I.L.; G.S.P.; R.B.; G.K.; formal analysis; G.S.P.; I.I.; V.X.; I.L.; investigation; I.L.; G.S.P.; R.B.; G.K.; resources; G.K.; R.B.; I.I.; G.S.P.; M.B.; A.V.; data curation; G.S.P.; I.L.; I.I.; V.X.; R.B.; G.K.; writing—original draft preparation; I.L.; G.S.P.; I.I.; V.X.; writing—review and editing; I.L.; G.S.P.; I.I.; V.X.; visualization; I.L.; G.S.P.; I.I.; V.X.; M.B.; A.V.; supervision; I.L.; G.S.P.; I.I.; R.B.; G.K.; project administration; I.L.; funding acquisition; R.B. All authors have read and agreed to the published version of the manuscript."

Compliance with ethical standards

Funding

This study was partially funded by the Australia-India Council, Canberra, and the Indian Council of Historical Research, New Delhi.

Ethical approval

This article does not contain any studies with human participants or animals performed by any of the authors.

Declaration of competing interest

The authors declare that they have no known competing financial interests or personal relationships that could have appeared to influence the work reported in this paper.

Data availability

Data will be available upon request.

Acknowledgements

We thank the Director General, Archaeological Survey of India, New Delhi; and the Commissioner, Directorate of Archaeology and Museums, Government of Madhya Pradesh, Bhopal, for granting us permission for sampling at Daraki-Chattan. We are also grateful to Dr Arakhita

Pradhan, Mr Ram Krishna and Dr Manoj Kumar Rathore for helping us to secure the samples (for IL); and to Prof. R.G. Roberts for helping with OSL analyses in 2004. Ioannis Liritzis is thankful for the support of Sino-Hellenic Academic Project from Key Research Institute of Yellow River Civilization and Sustainable Development & Collaborative Innovation Center on Yellow River Civilization of Henan Province, Henan University, China. IL and AV thank M. Bratitsi for assistance in sampling and taken photos. We also thank the Australia-India Council, Canberra, and the Indian Council of Historical Research, New Delhi, for funding support of the rock art project.

References

Ageby, L., Angelucci, D.E., Brill, D., Carrer, F., Brückner, H., Klasen, N., 2022. Dating dry-stone walls with rock surface luminescence: a case study from the Italian Alps. J. Archaeol. Sci. 144, 105625.

Aitken, M.J., 1985. Thermoluminescence Dating. Academic Press.

Aitken, M.J., 1998. An Introduction to Optical Dating: the Dating of Quaternary Sediments by the Use of Photon-Stimulated Luminescence. Oxford Science Publications.

Banerjee, D., Murray, A.S., Bøtter-Jensen, L., Lang, A., 2001. Equivalent dose estimation using a single aliquot of polymineral fine grains. Radiat. Meas. 33 (1), 73–94.

Beaumont, P.B., Bednarik, R.G., 2013. Tracing the emergence of palaeoart in sub-Saharan Africa. Rock Art Research 30 (1), 33–54.

Bednarik, R., Kumar, G., Watchman, A.L., Roberts, R.G., 2005. Preliminary results of the EIP project. Rock Art Research 22 (2), 147–197.

Bednarik, R.G., Li, F., 1991. Rock art dating in China: past and future. Artifact 14, 25–33.

Bednarik, R.G., 1993. Palaeolithic art in India. Man Environment 18 (2), 33–40.

Bøtter-Jensen, L., Bulur, E., Duller, G.A.T., Murray, A.S., 2000. Advances in luminescence instrument systems. Radiat. Meas. 32, 523–528.

Brill, D., May, S.M., Mhammdi, N., King, G., Lehmann, B., Burow, C., Wolf, D., Zander, A., Brückner, H., 2021. Evaluating optically stimulated luminescence rock surface exposure dating as a novel approach for reconstructing coastal boulder movement on decadal to centennial timescales. Earth Surf. Dyn. 9, 205–234.

Brown, N.B., Moon, S., 2019. Revisiting erosion rate estimates from luminescence profiles in exposed bedrock surfaces using stochastic erosion simulations. Earth Planet Sci. Lett. 528, 115842, 2019.

Brinkiene, K., Česniene, J., Kalpokaite-Dickuviene, R., Lukosiute, I., 2016. Performance evaluation of refractory composite coatings in potassium rich environment. Mater. Sci. 22 (3), 451–457.

Chapot, S., Sohbati, R., Murray, A.S., Pederson, J.L., Rittenour, T.M., 2012. Constraining the age of rock art by dating a rockfall event using sediment and rock-surface luminescence dating techniques. Quat. Geochronol. 13, 18–25.

Du, Y.J., Hayashi, S., Liu, S.Y., 2005. Experimental study of migration of potassium ion through a two-layer soil system. Environ. Geol. 48, 1096–1106.

Durcan, J.A., King, G.E., Duller, G.A.T., 2015. DRAC: dose rate and age calculator for trapped charge dating. Quat. Geochronol. 28, 54–61.

Freiesleben, T., Sohbati, R., Murray, A.S., Jain, M., al Khasawneh, S., Hvidt, S., Jakobsen, B., 2015. Mathematical model quantifies multiple daylight exposure and burial events for rock surfaces using luminescence dating. Radiat. Meas. 81, 16–22.

Galli, A., Panzeri, L., Rondini, P., Poggiani Keller, R., Martini, M., 2020. Luminescence dating of rock surface. The case of monoliths from the megalithic sanctuary of ossimo-pat (Valle Camonica, Italy). Appl. Sci. 10, 7403.

Gliganic, L.A., Meyer, M.C., Sohbati, R., Jain, M., Barrett, S., 2019. OSL surface exposure dating of a lithic quarry in Tibet: laboratory validation and application. Quat. Geochronol. 49, 199–204.

Greilich, S., Wagner, G.A., 2009. Light thrown on history – the dating of stone surfaces at the geoglyphs of Palpa using OSL. In: Reideland, M., Wagner, G.A. (Eds.), New Technologies for Archaeology Multidisciplinary Investigations in Palpa and Nasca, Peru. Springer-Verlag, pp. 271–283.

Habermann, J., Schilles, T., Kalchgruber, R., Wagner, G.A., 2000. Steps towards surface dating using luminescence. Radiat. Meas. 32 (5), 847–851.

Hashimoto, T., Katayama, H., Sakaue, H., Hase, H., Arimura, T., Ojima, T., 1997. Dependence of some radiation-induced phenomena from natural quartz on hydroxyl-impurity contents. Radiat. Meas. 27 (2), 243–250.

Hashimoto, T., Notoya, S., Arimura, T., Konishi, M., 1996. Changes in luminescence colour images from quartz slices with thermal annealing treatments. Radiat. Meas. 26 (2), 233–242.

Ikeya, M., 1993. New Applications of Electron Spin Resonance: Dating, Dosimetry, and Microscopy. World Scientific.

Iliopoulos, I., Xanthopoulou, V., Tsolis-Katagas, P., 2011. A petrographic assessment of houseware and storage pithoi in the Early Helladic settlement of Helike, Achaia, Greece. In: Katsonopoulou, D. (Ed.), Helike IV, Protohelladika: Helike and Aigialeia: the Southern Greek Mainland. The Helike Society, pp. 127–142.

Jackman, A.P., Walters, R.A., Kennedy, V.C., 1984. Transport and concentration controls for chloride, strontium, potassium and lead in Uvas Creek, a small cobble-bed stream in Santa Clara county, California, U.S.A., 2. Mathematical Modeling Journal of Hydrology 75, 111–141.

Kitis, G., Kiyak, N.G., Polymeris, G.S., 2015. Temperature lags of luminescence measurements in a commercial luminescence reader. Nucl. Instrum. Methods Phys. Res. Sect. B Beam Interact. Mater. Atoms 359, 60–63.

Korisettar, R., 2002. In: Settar, S., Korisettar, R. (Eds.), Prehistory. Archaeology of south Asia, Indian Archaeology in Retrospect, 1. Indian Council of Historical Research, Manohar, pp. 1–65.

Krishna, R., Kumar, G., 2016. Understanding the Technology of Very Small Cupules in Daraki-Chattan, India. In: Kumar, G., Bednarik, R.G., Fiore, D., Basile, M., Huisheng, T. (Eds.), Paleoart and Materiality: the Scientific Study of Rock Art, pp. 187–194.

Kumar, G., Krishna, R., 2015. Manual of Cupule Replication Technology. Arts 4, 101–120.

Laskaris, N., Liritzis, I., 2011. A new mathematical approximation of sunlight attenuation in rocks for surface luminescence dating. J. Lumin. 131 (9), 1874–1884.

Li, S.-H., Li, B., 2019. Advances in Physics and Applications of Optically and Thermally Stimulated Luminescence. In: Chen, R., Pagonis, V. (Eds.), Advances in Physics and Applications of Optically and Thermally Stimulated Luminescence. World Scientific, pp. 363–398.

Liritzis, I., 1994(a). A new dating method by thermoluminescence of carved megalithic stone building. Computes Rendus - Academie des Sciences, Serie II: Sciences de la Terre et des Planetes 319, 603–610.

Liritzis, I., 1994(b). Archaeometry: Dating the past. EKISTICS 368/364, 361–366.

Liritzis, I., 2011. Surface dating by luminescence: an overview. Geochronometria 38 (3), 292–302.

Liritzis, I., 2022. Optically stimulated luminescence dating using quartz: remarks and a plea for fairness. Scientific Culture 8 (1), 175–194.

Liritzis, I., Bednarik, R., Kumar, G., Polymeris, G.S., Iliopoulos, I., Xanthopoulou, V., Zacharias, N., Vafiadou, A., Bratitsi, M., 2019. Daraki-Chattan rock art constrained OSL chronology and multi analytical techniques: A first pilot investigation. J. Cult. Herit. 37, 29–43.

Liritzis, I., Galloway, R.B., 1999. Dating implications from solar bleaching of thermoluminescence of ancient marble. J. Radioanal. Nucl. Chem. 241 (2), 361–368.

Liritzis, I., Kitis, G., Galloway, R.B., Vafiadou, A., Tsirliganis, N., Polymeris, G., 2008. Probing luminescence dating of archaeologically significant carved rock types. Mediterranean Archaeology & Archaeometry 8 (1), 61–79.

Liritzis, I., Panou, E., Exarhos, M., 2017. Novel approaches in surface luminescence dating of rock art: a brief review. Mediterranean Archaeology and Archaeometry 17 (4), 89–102.

Liritzis, I., Singhvi, A.K., Feathers, J.K., Wagner, G.A., Kadereit, A., Zacharias, N., Li, S.-H., 2013. Luminescence Dating in Archaeology, Anthropology and Geoarchaeology: an Overview. Springer.

Liritzis, I., Vafiadou, A., 2012. Calibration aspects of thick source alpha counter ZnS system. Measurement 45 (8), 1966–1980.

Liritzis, I., Polymeris, G., Zacharias, N., 2010. Surface luminescence dating of 'Dragon Houses' and Armena Gate at Styra (Euboea, Greece). Mediterranean Archaeology & Archaeometry, Special Issue, (D.Keller, guest editor) 10 (No.3), 65–81.

Liritzis, I., Stamoulis, K., Papachristodoulou, Ch, Ioannides, K.G., 2013b. A re-evaluation of radiation dose rate conversion factors. Mediterr. Archaeol. Archaeometry 13 (3), 1–15.

Liritzis, I., Aravantinos, G.S.V., Polymeris, N., Zacharias, I., Fappas, G., Agiamarniotis, I. K. Sfampa, Vafiadou, A., Kitis, G., 2015. Witnessing prehistoric Delphi by Luminescence dating. Comptes Rendus Palevol 14, 219–232.

Liritzis, I., Vafiadou, A., 2015. Surface luminescence dating of some Egyptian monuments. J. Cult. Herit. (2), 134–150.

Liritzis, I., Vafiadou, A., Zacharias, N., Polymeris, G.S., Bednarik, R., 2013(c). Advances in surface luminescence dating: some new data from three selected Mediterranean sites. Mediterranean Archaeology and Archaeometry 13 (3), 105–115.

Liritzis, I., Miller, M.C., Alappat, L., 2020(a). The value of OSL in distinguishing ancient from more recent structures in an archaeological landscape. Scientific Culture 6 (No. 2), 23–34. https://doi.org/10.5281/zenodo.3724844.

Liritzis, I., Laskaris, N., Vafiadou, A., Karapanagiotis, I., Volonakis, P., Papageorgopoulou, C., Bratitsi, M., 2020(b). Archaeometry: an overview. Scientific Culture 6 (No. 1), 49–98. https://doi.org/10.5281/zenodo.3625220.

McKeever, S.W.S., 1984. Thermoluminescence in quartz and silica. Radiat. Protect. Dosim. 8 (1–2), 81–98.

McKeever, S.W.S., 1985. Thermoluminescence of Solids. Cambridge University Press.

Mediterranean Archaeology and Archaeometry (MAA), 2017. Special Issue on Rock Art 17 (4). http://www.maajournal.com/Issues2017d.php.

Mishra, S., 1992. The age of the Acheulian in India: new evidence. Curr. Anthropol. 33, 325–328.

Murray, M.S., Wintle, A.G., 2000. Luminescence dating of quartz using an improved single-aliquot regenerative-dose protocol. Radiat. Meas. 32, 57–73.

Olley, J., Caitcheon, G., Murray, A.S., 1998. The distribution of apparent dose as determined by Optically Stimulated Luminescence in small aliquots of fluvial quartz: Implications for dating young sediments. Quat. Sci. Rev. 17, 1033–1040.

Ou, X.J., Roberts, H.M., Duller, G.A.T., Gunn, M.D., Perkins, W.T., 2018. Attenuation of light in different rock types and implications for rock surface luminescence dating. Radiat. Meas. 120, 305–311.

Paddayya, K., 1991. The Acheulian culture of the Hunsgi and Baichbal valleys, peninsular India: a processual study. Quartär 41/42, 111–138.

Pinnioja, S., 1998. Thermoluminescence method for detection of irradiated food. In: Report Series in Radiochemistry, 9/1998. University of Helsinki, PhD.

Polykreti, K., Michael, C.T., Maniatis, Y., 2002. Authenticating marble sculptures using thermoluminescence. Ancient TL 20 (1), 11–18.

Polymeris, G.S., Giannoulatou, V., Kyriakidou, A., Sfampa, I.K., Theodorou, G.S., Şahiner, E., Meriç, N., Kitis, G., Paraskevopoulos, K.M., 2017. Bioactivity characterization of 45S5 bioglass using TL, OSL and EPR: Comparison with the case of 58S sol-gel bioactive glass. Mater. Sci. Eng. C 70, 673–680.

Polymeris, G.S., Goudouri, O.M., Paraskevopoulos, K.M., Kitis, G., 2012. The 110 °C thermoluminescence as a probe in bioactivity studies; the case of 58S sol–gel bioactive glass. Key Eng. Mater. 493, 494 49–54.
Poolton, N.R.J., Bøtter-Jensen, L., Johnsen, O., 1996. On the relationship between luminescence excitation spectra and feldspar mineralogy. Radiat. Meas. 26 (1), 93–101.
Raghvan, H., Rajaguru, S.N., Misra, V.N., 1989. Radiometric dating of a Quaternary dune section, Didwana, Rajasthan. Man Environ. 13, 19–22.
Rogers, J.J.W., Richardson, K.A., 1964. Thorium and uranium contents in some sandstones. Geochem. Cosmochim. Acta 28 (12), 2005–2011.
Scarre, C., 2010. Rocks of ages: tempo and time in megalithic monuments. Eur. J. Archaeol. 13 (2), 175–193.
Schmidt, K., Linemann, H., Giessing, R., 1974. Influences of preparation and annealing on the properties of $CaSO_4$:Dy thermoluminescence phosphor. In: Niewiadomski, T. (Ed.), Proceedings of the Fourth International Conference on Luminescence Dosimetry. Institute of Nuclear Physics, pp. 237–253. Kraków, Poland, 27-31 August, 1974.
Sellwood, E.L., Kook, M., Jain, M., 2022. Rapid in-situ assessment of luminescence bleaching depths in rocks for deriving burial and exposure chronologies of rock surfaces. Quat. Geochronol. 67, 101227.
Smedley, R.K., Small, D., Jones, R.S., Brough, S., Bradley, J., Jenkins, G.T.H., 2021. Erosion rates in a wet, temperate climate derived from rock luminescence techniques. Geochronology 3, 525–543. https://doi.org/10.5194/gchron-3-525-2021.
Sohbati, R., 2013. Luminescence, Rock Surfaces. In: Rink, W., Thompson, J. (Eds.), Encyclopedia of Scientific Dating Methods. Springer.
Sohbati, R., Murray, A.S., Chapot, M.S., Jain, M., Pederson, U., 2012. Optically stimulated luminescence (OSL) as a chronometer for surface exposure dating. J. Geophys. Res. 117, B09202.
Sohbati, R., Murray, A.S., Porat, N., Jain, M., Avner, U., 2015. Age of a prehistoric "Rodedian" cult site constrained by sediment and rock surface luminescence dating techniques. Quat. Geochronol. 30, 90–99.
Szabo, B.J., McKinney, C., Dalbey, T.S., Paddayya, K., 1990. On the age of the Acheulian culture of the Hunsgi-Baichbal valleys, peninsular India. Bull. Deccan Coll. Postgrad. Res. Inst. 50, 317–321.
Townsend, P.D., Maghrabi, M., Yang, B., 2002. Luminescence detection of phase transitions. Nucl. Instrum. Methods B 191, 767–771.
Townsend, P.D., Yang, B., Wang, Y., 2008. Luminescence detection of phase transitions, local environment and nanoparticle inclusions. Contemp. Phys. 49 (4), 255–280.
Van Peer, P., Fullager, R., Stokes, S., Bailey, R.M., Moeyersons, J., Steenhoudt, F., Geerts, A., Vanderbeken, T., De Dapper, N., Geus, F., 2003. The Early to Middle Stone Age transition and the emergence of modern behaviour at site 8-B-11, Sai Island, Sudan. J. Hum. Evol. 45 (2), 187–193.